purpose for which the variables were used (Table 2). For example, if the optimal thresholds of the integral values of R1 and R2 derived from the initial site (73 and 104) were applied to the independent test data from the remaining 6 sites, the sensitivities were 0.73 (proportion of patients/measurement: 96/131) and 0.79 (104/131) and the specificities were 0.63 (proportion of HCs/measurement: 326/514) and 0.63 (324/514) for R1 (positive predictive value (PPV) = 0.37, negative predictive value (NPV) = 0.90) and R2 (PPV = 0.40, NPV = 0.92), respectively.

Test for differentiation of patients with unipolar MDD from those with BP and SZ

Using the preliminary data from the initial site, one-way ANOVA performed between the patients with MDD and those with one of the other 2 disorders of interest (BP or SZ) revealed a significant difference in the R1 centroid values [$F(1,53) = 9.54$, $p < 0.01$; $d = 0.96$, 95% CI, (0.25 to 1.62)], but not in the R1 [$F(1,53) = 0.14$, $p = 0.71$] or the R2 [$F(1,53) = 0.05$, $p = 0.83$] integral values.

As the significant R1 centroid value proved to be the most useful variable, we applied it to ROC analysis for the differentiation of patients with unipolar MDD from those with non-MDD disorders. The resulting area under the ROC curve (Az) value was 0.74 [95% CI, (0.61 to 0.87)] and the optimal threshold was 54 [s] from the extreme top left point of the ROC curve (eFig. S4).

To validate the optimal threshold calculated, we applied it to the independent test data of the remaining 6 sites, to differentiate the patients with MDD from those with SZ and BP [Az = 0.81, 95% CI, (0.74 to 0.89); $d = 1.17$, 95% CI, (0.79 to 1.54); optimal threshold = 54 [s], PPV = 0.79, NPV = 0.82; Fig. 4]. Using this threshold (54 [s]), 74.6% of the patients with MDD (proportion of patients/measurement: 41/55) and 85.5% of those with SZ or BP (65/76) were classified correctly [76.9% of BP patients (20/26) and 90.0% of SZ patients (45/50)] (Fig. 5). The ROC curves of MDD v. BP [Az = 0.74, 95% CI, (0.62 to 0.85); $d = 0.81$, 95% CI, (0.32 to 1.29); optimal threshold = 54 [s], PPV = 0.87, NPV = 0.59] and MDD v. SZ [Az = 0.86, 95% CI, (0.78 to 0.93); $d = 1.40$, 95% CI, (0.96 to 1.82); optimal threshold = 54 [s], PPV = 0.89, NPV = 0.78] are shown separately in eFig. S5.

For reference, the test performed for the differentiation between patients with BP and those SZ is shown in Supplementary Material (VII).

Correlational analysis of demographic and clinical confounding factors

Correlational analysis showed no significant correlations between any of the significant dependent variables (among the R1 and R2 integral values and the R1 centroid value of NIRS signals) and any of the demographic confounding factors [performance (number of correct words), education years and pre-morbid IQ; $p > 0.05$] for all patients with psychiatric disorders (MDD, BP and SZ).

Regarding clinical confounding factors, a stepwise regression analysis of each significant dependent variable for each disorder revealed that there was no entry clinical variable in the linear regression models, with the exception of the global assessment of functioning (GAF) score (beta = 0.50, $p < 0.01$) for the R2 integral value ($F = 10.73$, $p < 0.01$; $R = 0.50$, $R^2 = 0.25$, adjusted $R^2 = 0.23$) in patients with MDD, and the GAF score (beta = 0.58, $p = 0.01$) for the R2 integral value ($F = 8.43$, $p = 0.01$; $R = 0.59$, $R^2 = 0.35$, adjusted $R^2 = 0.30$) in patients with BP who exhibited depressive symptoms. Thus, only one clinical variable (i.e., GAF score) among all of the medication and clinical variables examined had a significant impact on the R2 integral values for patients with MDD or BP who exhibited depressive symptoms.

Table 2
Sensitivities and specificities of the integral values of Region 1 (R1) and Region 2 (R2) signals between healthy controls and all patients with psychiatric disorders, based on the independent data collected from the 6 additional sites.

Integral value	R1		R2	
	Sensitivity	Specificity	Sensitivity	Specificity
160	0.95	0.27	0.90	0.39
150	0.93	0.30	0.89	0.43
140	0.92	0.34	0.88	0.47
130	0.90	0.37	0.87	0.52
120	0.88	0.42	0.85	0.57
110	0.85	0.46	0.82	0.61
100	0.82	0.50	0.78	0.64
90	0.78	0.54	0.76	0.68
80	0.74	0.61	0.73	0.73
70	0.72	0.65	0.64	0.76
60	0.66	0.71	0.57	0.78
50	0.57	0.75	0.52	0.81
40	0.47	0.80	0.43	0.86
30	0.38	0.84	0.33	0.89

Discussion

The present multi-site study is the first large-scale, case–control study that demonstrates the utility of NIRS for the differential diagnosis of major psychiatric disorders. The main strengths of this study include the application of a neuroimaging biomarker in clinical practice that allows the clinically useful differential diagnosis of depressive states. The frontal centroid value, which represents the timing of frontal NIRS signal patterns, was a significant variable for differential diagnosis and the optimal threshold derived from the ROC analysis correctly discriminated patients with unipolar MDD (74.6%) from those with non-MDD disorders (85.5%; BP, 76.9% and SZ, 90.0%).

Single-individual diagnostic classification analyses among various psychiatric disorders

The present study was not only a case–control study of group comparisons, but also a study specifically designed for examining the practical utility of single-individual diagnostic classification in various psychiatric disorders. Several studies have reported the single-individual diagnostic classification of one psychiatric disorder compared with HCs by applying multivariate statistical methods (e.g.,

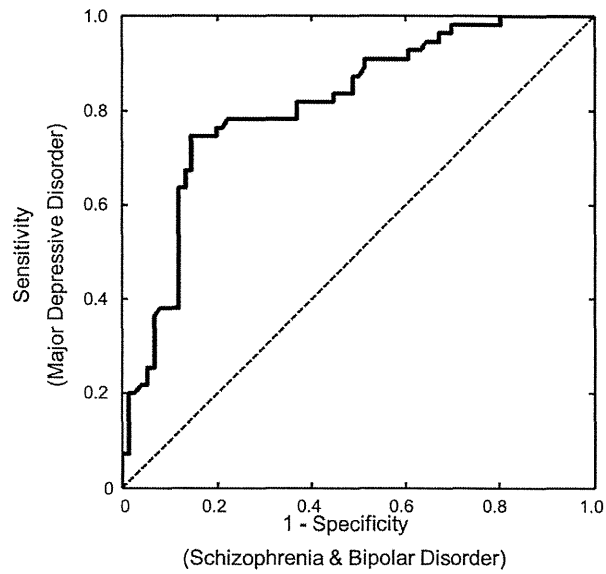

Fig. 4. Receiver operating characteristic analysis of the centroid value of Region 1 (R1) near-infrared spectroscopy signal between patients with major depressive disorder and those with either of the other 2 disorders of interest (bipolar disorder and schizophrenia) based on the independent data collected from the 6 additional sites.

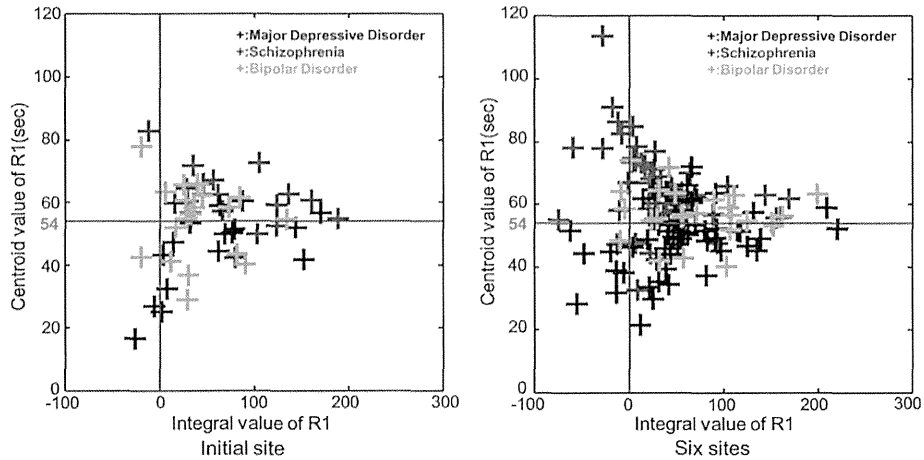

Fig. 5. Scatter plots of the centroid and integral values of Region 1 (R1) signal in the patients, both at the initial site (Gunma University) and at the 6 additional sites.

neuroanatomical pattern classification) to structural MRI data (Davatzikos et al., 2005) and NIRS data (Hahn et al., 2013) from SZ and high-risk psychosis samples (Koutsouleris et al., 2009), as well as to functional MRI data from patients with depression (Hahn et al., 2011). These studies were technically sophisticated; however, more research must be performed to test their reproducibility and generalisability in the advanced stage of clinical application, because (1) they were designed for the analysis of one diagnostic classification based on comparison to HCs, and not for differential diagnosis among multiple psychiatric disorders; and (2) they were performed using one relatively small cohort; thus, they must be replicated in another cohort including larger sample groups.

Furthermore, we will discuss briefly our results in comparison with those of other single-individual diagnostic classification studies (Davatzikos et al., 2005; Fu et al., 2008; Hahn et al., 2011; Koutsouleris et al., 2009). We used only a single variable (simple 'centroid value' of NIRS signals) and found that the classification rates (unipolar MDD: 74.6% correct classification; the 2 other disorders: 85.5% correct classification (BP, 76.9%; SZ, 90.0%)) were almost equivalent to the rates reported in the previous MRI studies using multivariate statistical methods (which had 80–90% classification rates in the patient group compared with the HC group).

To determine whether a higher disease classification rate could be achieved by using a multivariate pattern analysis (compared with that obtained using one simple variable), which was used in previous MRI studies, we confirmed the results using the multivariate pattern classification analysis described in Supplementary Material (VIII). The leave-one-out cross-validation method revealed that 4 significant variables, or even one variable (the R1 centroid value), could differentiate patients with unipolar MDD from those with either of the 2 other disorders (non-MDD) with a similar degree of mean accuracy (76.8% (unipolar MDD: 73.0% (54/74), non-MDD: 74.8% (83/111))).

Clinical importance and implications

Another clinically valuable feature of our work is that it aimed to facilitate diagnosis among patients with similar depressive symptoms, which psychiatrists often find to be a difficult task. Most BP patients with depressive symptoms are initially diagnosed with and treated for MDD (Akiskal et al., 1995; Goldberg et al., 2001). Therefore, our findings may help differentiate BP with depressive symptoms from MDD. Depressive symptoms and cognitive deficits are also common early signs of SZ (Hafner et al., 2005). Of particular clinical relevance is the observation that SZ patients with concomitant depression have a greater risk of suicide or an unfavourable disease course (an der Heiden et al., 2005). Therefore, sufficient attention must be given to the diagnosis and treatment of depression in SZ patients.

The results of the present study may draw attention to the heterogeneity observed among MDD patients. Rather than simply being misclassified, approximately 25% of patients with unipolar MDD who were classified by the system as having a non-MDD disorder may have a brain pathophysiology that is biologically different from that of the majority of MDD patients. Evidence suggests that 25–50% of individuals with recurrent major depression (particularly those in atypical early-onset or treatment-refractory subgroups) may in fact have broadly defined BP (Angst, 2007). In this study, 74.6% of the patients with MDD were classified correctly; the remaining 25.4% might include either patients who would progress to a diagnosis of one of the 2 other disorders or patients with a broadly defined BP who were diagnosed with MDD according to the DSM criteria. This explanation might be justified by the finding of a correct classification rate of 75% for patients with MDD. For practical purposes, among patients diagnosed clinically with MDD, the early suspicion of the possibility of a diagnosis of a non-MDD disorder with depression would also provide an opportunity to reduce the hazardous effects of the illness on personal, social and occupational aspects; therefore, our results should be of great clinical importance in practical applications. Thus, a prospective study aimed at elucidating the heterogeneity of unipolar MDD is required.

Advantages of the NIRS method

We used the same NIRS system (a non-invasive, portable and user-friendly device) and the same concise measurement procedure at every site; therefore, inter-site compatibility was not an issue here; however, it may be an obstacle in other neuroimaging multi-site studies. Furthermore, we used a high temporal resolution (0.1 s) in the NIRS system for measuring time-specific characteristics of dynamic prefrontal cortical functions; this enabled analyses that included more detailed time-course comparisons of NIRS signal changes. We created and adopted new variables, such as the 'centroid value', to determine the timing of the haemodynamic response (Fig. 1). The high temporal resolution of NIRS might allow not only the detection of functional abnormalities (e.g., hypofrontality), but also the capture of the specific haemodynamic activation time courses of each psychiatric disorder and aid differential diagnosis.

The practical application of biomarkers requires that they be relatively simple. The simplicity of both the test procedure and the associated data analysis is important not only for the participants, but also for their caretakers and clinicians. Therefore, rather than using complicated multivariate statistical methods, we developed a robust classification algorithm for real-time visual evaluation of patients using the simplest, and lowest number of variables on the basis of a ROC analysis. This was important because we sought to develop a psychiatric practice empowered by the initiative of patients by sharing the 'comprehensively visualised' results that can be easily recognisable by patients and caretakers, rather than results from complicated 'black-box' analyses. In addition, using the condensed VFT (<3 min) developed previously by us, we designed a diagnostic support system in a way that the results are available to clinicians in less than 15 min. The availability of such a 'comprehensively visualised' report to clinicians, patients and their caretakers at a first visit, while laying out a future treatment plan, would likely lead to a paradigm shift to a patient-centred approach in clinical psychiatry.

Limitations

The methodological aspects of the present study warrant commentary. First, most of the patients included in the study were taking medications at the time of measurement. To our knowledge, no clear evidence of the effects of medication on NIRS signals has been demonstrated. We found that none of the medications at any dose was significantly correlated with NIRS signals in this study; however, we cannot fully exclude the effects of medication on haemodynamic signals. For confirmation, the application of the algorithm described above (optimal cut-off of the R1 centroid value) to the drug-free patients exclusively, 6 out of 10 patients with MDD patients (60%) and 4 out of 5 patients with SZ (80%) were classified correctly. Second, the size of the sample included in our final analysis was substantially reduced from that initially recruited, because we tried to minimise the confounding factors of age and gender by matching the groups and excluded patients in remission, as well as patients in the manic phase (see Flow diagram). In our confirmatory analysis, we included all non-matched and in-remission patients and found that the results were quite similar, although this analysis had a lower detection power. The optimal threshold of the sample sets before demographical matching was also the same as that calculated originally. These results suggest that the reduction in the total number of study participants after demographical matching did not affect the development of the algorithm [see Supplementary Material (I)]. However, we must consider the possibility that this diagnostic support system is best suited for young and middle-aged patients with moderate or severe symptoms (e.g., aged between 23 and 65 years (mean $\pm$ 1.5 SD)). Third, a PCA of haemodynamic response performed to capture a channel cluster led to the identification of 2 cluster regions. Nonetheless, as we thought that pooling many NIRS signals together into only 2 representative regions of interest (R1 (frontopolar and dorsolateral prefrontal regions) and R2 (ventrolateral prefrontal and temporal regions)) might oversimplify the results (see the Discussion of Supplementary Material (II)), we sought to confirm the reliability of the 2 clusters by performing a test–retest analysis in a portion of the samples. We found significant ICCs for both the R1 and R2 integral values and for the R1 centroid value between 2 measurements (see Supplementary Material (IV)). Therefore, we used the two data-derived clusters that reflected a fronto-temporal haemodynamic response during VFT. Fourth, we have controlled some well-known confounders in the analyses. However, the NIRS signal might be affected by the other systemic confounders, such as autonomic function, neuroendocrine function, diet and physical activity. In addition, brain anatomical factors, such as scalp–cortex distance and frontal sinus volume, as well as genetic variants might also be potential confounders. Further studies are required to address the relationship between the NIRS signal and these confounders. If these findings are fully replicated, the development of methods of integrating confounding factors into NIRS signal in the future will be ideal. Fifth, we did not use the exclusion criterion of first-degree relatives with axis I psychiatric disorders for healthy controls. This could give a bias to the data in healthy controls, which means that some of the first-degree relatives of persons with axis I psychiatric disorders might have been included as a healthy control in the present study. However, as the same situations are assumed in real clinical settings, we daringly recruited healthy controls without applying that strict exclusion criterion.

Conclusions and future implications

In conclusion, this multi-site study provided evidence that the fronto-temporal NIRS signal may be used as a tool in assisting the diagnosis of major psychiatric disorders with depressive symptoms. Future NIRS research should be performed to study the applicability of this method to (1) the identification of a need for therapy, (2) the assessment of the efficacy of various treatments, (3) the establishment of prognostic predictions that may be clarified by longitudinal follow-up assessments of patients in various clinical stages and (4) the examination of the use of NIRS as a screening tool.

Supplementary data to this article can be found online at http://dx.doi.org/10.1016/j.neuroimage.2013.05.126.

Acknowledgments

The authors would like to thank all the participants in this study. The authors also thank Makoto Ito, M.D., Ph.D., Tomohiro Suto, M.D., Ph.D., Yutaka Yamagishi, M.D., Naoki Hanaoka, M.D., Ph.D., Toshimasa Sato, Ed.M. and Noriko Sakurai of Gunma University; Kohei Marumo, M.D., Ph.D. and Yuki Kawakubo, Ph.D., of The University of Tokyo; Hitomi Kobayashi, Ph.D. and Junko Motoki, Ph.D., of Showa University; Osamu Saitoh, M.D., Ph.D., Kimitaka Anami, M.D., Ph.D., Yohtaro Numachi, M.D., Ph.D., Yuji Sugimura and Masaru Ogawa of the National Centre of Neurology & Psychiatry Hospital; Daisuke Gotoh, M.D., Yojiro Sakai, M.D., Ph.D. and Emi Yoshida, M.D., of Fukushima Medical University, for technical assistance during data collection.

Role of the funding source

This study was supported in part by grants-in-aid for scientific research from the Japan Society for the Promotion of Science (JSPS) and the Ministry of Education, Culture, Sports, Science, and Technology (MEXT) of Japan (Nos. 18390318, 19659289, 20390310 and 22659209 to MF; Nos. 21249064 and 221S003 [Innovative Areas (Comprehensive Brain Science Network)] to KK; No. 17019029 [Priority Areas (Applied Genomics)] to YO; and No. 23791309 to RT), and by grants-in-aid from the Ministry of Health, Labour, and Welfare (MHLW) of Japan (H20-kokoro-ippan-001, H20-3, and H22-seishin-ippan-015 to KK). This study was also supported in part by Health and Labour Sciences Research Grants for Comprehensive Research on Disability Health and Welfare (previously, Health and Labour Science Research Grant for Research on Psychiatric and Neurological Disease and Mental Health; H20-001 to MF and H23-seishin-ippan-002 to RT) and by the Intramural Research Grants for Neurological and Psychiatric Disorders of The National Centre of Neurology and Psychiatry (previously, The Research Grant for Nervous and Mental Disorders from the MHLW; 21B-1 to MF and 20B-3 to TN). In addition, this study was supported in part by an Intramural Research Grant for Neurological and Psychiatric Disorders of NCNP (No. 23-10 to RT). A part of this study was also the result of a project entitled 'Development of biomarker candidates for social behavior', which was carried out under the Strategic Research Program for Brain Sciences by MEXT, Japan. This study was also supported in part

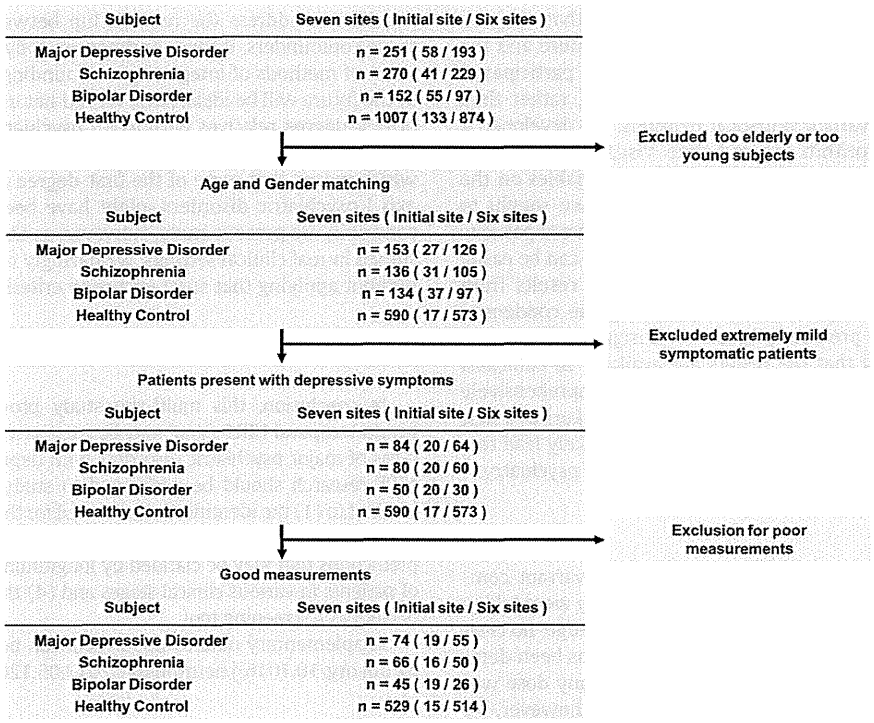

Flow diagram. Main analyses were based on matched samples according to the flow diagram.

by grants from the Japan Research Foundation for Clinical Pharmacology (to RT).

The funders had no role in the design of the study, data collection, data analysis, decision to publish, or preparation of the manuscript. The corresponding author had full access to all of the data in this study and takes responsibility for the integrity of the data, the accuracy of the data analysis and the decision to submit the manuscript for publication.

Author contributions

Masato Fukuda designed the experiments and organized the multi-site collaborative study. Ryu Takizawa, Masato Fukuda, Shingo Kawasaki, and Kiyoto Kasai analysed the data and wrote the first draft of the paper. The other contributors performed data acquisition and revised the first draft critically for important intellectual content. All contributors have approved the final version of the manuscript.

Contributors from the Joint Project for Psychiatric Application of Near-Infrared Spectroscopy (JPSY-NIRS) Group

Gunma University: Masato Fukuda, M.D., Ph.D., Masashi Suda, M.D., Ph.D., Yuichi Takei, M.D., Ph.D., Yoshiyuki Aoyama, M.D., Ph.D., Kosuke Narita, M.D., Ph.D., Masahiko Mikuni, M.D., Ph.D., Masaki Kameyama, M.D., Ph.D., and Toru Uehara, M.D., Ph.D.

The University of Tokyo: Ryu Takizawa, M.D., Ph.D., Kiyoto Kasai, M.D., Ph.D., Masaru Kinou, M.D., Ph.D., Shinsuke Koike, M.D. and Ayaka Ishii-Takahashi, M.D.

Hitachi Medical Corporation: Shingo Kawasaki, MS, Noriyoshi Ichikawa, BS, and Michiyuki Fujiwara, AS.

Showa University: Haruhisa Ohta, M.D., Ph.D., Hiroi Tomioka, M.D., Ph.D., Bun Yamagata, M.D., Ph.D., and Kaori Yamanaka, M.D.

Keio University: Masaru Mimura, M.D., Ph.D.

Tottori University: Shenghong Pu, Ph.D.

The National Centre of Neurology and Psychiatry: Kazuyuki Nakagome, M.D., Ph.D., Takamasa Noda, M.D., Taro Matsuda, M.D., and Sumiko Yoshida, M.D., Ph.D.

Fukushima Medical University: Shin-Ichi Niwa, M.D., Ph.D., Soichi Kono, M.D., Hirooki Yabe, M.D., Ph.D., and Sachie Miura, M.D.

Mie University and Tokyo Metropolitan Matsuzawa Hospital: Yuji Okazaki, M.D., Yukika Nishimura, Ph.D., Hisashi Tanii, M.D., Ph.D., Ken Inoue, M.D., Ph.D., Chika Yokoyama, MA, Yoichiro Takayanagi, M.D., Ph.D., Katsuyoshi Takahashi, M.D., and Mayumi Nakakita, M.D.

Conflict of interest

We would like to disclose potential conflicts of interest regarding all financial and material support for the present study. The principal investigators of each site (Masato Fukuda of Gunma University, Kiyoto Kasai of The University of Tokyo, Masaru Mimura of Keio university and Showa University, Kazuyuki Nakagome of The National Center of Neurology and Psychiatry and Tottori University, Shin-ichi Niwa of Fukushima Medical University, Yuji Okazaki of both Mie University and Tokyo Metropolitan Matsuzawa Hospital and Takamasa Noda of The National Center of Neurology and Psychiatry) have potential conflicts of interest in the submitted work. Each site has had an official contract with the Hitachi Group (Advanced Research Laboratory, Hitachi, Ltd., and The Research and Developmental Center, Hitachi Medical Corporation) for a collaborative study of the clinical application of NIRS in psychiatric disorders. For this study, the Hitachi Group provided a project grant (JPY 300,000–2,000,000 per year) and material support (temporary rental of a NIRS (Optical Topography) ETG-4000 system) for each site. Shingo Kawasaki, Noriyoshi Ichikawa and Michiyuki Fujiwara are employees of Hitachi Medical Corporation.

The other authors have no financial relationships with any organisations that might have an interest in the submitted work in previous years and no other relationships or activities that could appear to have influenced the submitted work.

References

Akiskal, H.S., Maser, J.D., Zeller, P.J., Endicott, J., Coryell, W., Keller, M., Warshaw, M., Clayton, P., Goodwin, F., 1995. Switching from 'unipolar' to bipolar II. An 11-year

prospective study of clinical and temperamental predictors in 559 patients. Arch. Gen. Psychiatry 52, 114–123.
Almeida, J.R., Versace, A., Mechelli, A., Hassel, S., Quevedo, K., Kupfer, D.J., Phillips, M.L., 2009. Abnormal amygdala–prefrontal effective connectivity to happy faces differentiates bipolar from major depression. Biol. Psychiatry 66, 451–459.
an der Heiden, W., Konnecke, R., Maurer, K., Ropeter, D., Hafner, H., 2005. Depression in the long-term course of schizophrenia. Eur. Arch. Psychiatry Clin. Neurosci. 255, 174–184.
Angst, J., 2007. The bipolar spectrum. Br. J. Psychiatry 190, 189–191.
Barch, D.M., Sheline, Y.I., Csernansky, J.G., Snyder, A.Z., 2003. Working memory and prefrontal cortex dysfunction: specificity to schizophrenia compared with major depression. Biol. Psychiatry 53, 376–384.
Barrett, S.L., Mulholland, C.C., Cooper, S.J., Rushe, T.M., 2009. Patterns of neurocognitive impairment in first-episode bipolar disorder and schizophrenia. Br. J. Psychiatry 195, 67–72.
Costafreda, S.G., Fu, C.H., Lee, L., Everitt, B., Brammer, M.J., David, A.S., 2006. A systematic review and quantitative appraisal of fMRI studies of verbal fluency: role of the left inferior frontal gyrus. Hum. Brain Mapp. 27, 799–810.
Curtis, V.A., Dixon, T.A., Morris, R.G., Bullmore, E.T., Brammer, M.J., Williams, S.C., Sharma, T., Murray, R.M., McGuire, P.K., 2001. Differential frontal activation in schizophrenia and bipolar illness during verbal fluency. J. Affect. Disord. 66, 111–121.
Davatzikos, C., Shen, D., Gur, R.C., Wu, X., Liu, D., Fan, Y., Hughett, P., Turetsky, B.I., Gur, R.E., 2005. Whole-brain morphometric study of schizophrenia revealing a spatially complex set of focal abnormalities. Arch. Gen. Psychiatry 62, 1218–1227.
Ferrari, M., Quaresima, V., 2012. A brief review on the history of human functional near-infrared spectroscopy (fNIRS) development and fields of application. Neuroimage 63 (2), 921–935.
First, M.B., Spitzer, R.L., Gibbon, M., Williams, J.B.W., 1997. Structured Clinical Interview for DSM-IV Axis I Disorders. Biometric Research Department, New York State Psychiatric Institute, New York, U.S.A.
Fu, C.H., Mourao-Miranda, J., Costafreda, S.G., Khanna, A., Marquand, A.F., Williams, S.C., Brammer, M.J., 2008. Pattern classification of sad facial processing: toward the development of neurobiological markers in depression. Biol. Psychiatry 63, 656–662.
Goldberg, J.F., Harrow, M., Whiteside, J.E., 2001. Risk for bipolar illness in patients initially hospitalized for unipolar depression. Am. J. Psychiatry 158, 1265–1270.
Gur, R.E., Keshavan, M.S., Lawrie, S.M., 2007. Deconstructing psychosis with human brain imaging. Schizophr. Bull. 33, 921–931.
Hafner, H., Maurer, K., Trendler, G., an der Heiden, W., Schmidt, M., 2005. The early course of schizophrenia and depression. Eur. Arch. Psychiatry Clin. Neurosci. 255, 167–173.
Hahn, T., Marquand, A.F., Ehlis, A.C., Dresler, T., Kittel-Schneider, S., Jarczok, T.A., Lesch, K.P., Jakob, P.M., Mourao-Miranda, J., Brammer, M.J., Fallgatter, A.J., 2011. Integrating neurobiological markers of depression. Arch. Gen. Psychiatry 68, 361–368.
Hahn, T., Marquand, A.F., Plichta, M.M., Ehlis, A.C., Schecklmann, M.W., Dresler, T., Jarczok, T.A., Eirich, E., Leonhard, C., Reif, A., Lesch, K.P., Brammer, M.J., Mourao-Miranda, J., Fallgatter, A.J., 2013. A novel approach to probabilistic biomarker-based classification using functional near-infrared spectroscopy. Hum. Brain Mapp. 34, 1102–1114.
Hamilton, M., 1960. A rating scale for depression. J. Neurol. Neurosurg. Psychiatry 23, 56–62.
Holsboer, F., 2008. How can we realize the promise of personalized antidepressant medicines? Nat. Rev. Neurosci. 9, 638–646.
Hoshi, Y., Kobayashi, N., Tamura, M., 2001. Interpretation of near-infrared spectroscopy signals: a study with a newly developed perfused rat brain model. J. Appl. Physiol. 90, 1657–1662.
Kameyama, M., Fukuda, M., Yamagishi, Y., Sato, T., Uehara, T., Ito, M., Suto, T., Mikuni, M., 2006. Frontal lobe function in bipolar disorder: a multichannel near-infrared spectroscopy study. NeuroImage 29, 172–184.
Kay, S.R., Opler, L.A., Fiszbein, A., 1991. Positive and Negative Syndrome Scale (PANSS) Rating Manual. Multi-health Systems Inc., Toronto.
Koike, S., Takizawa, R., Nishimura, Y., Takano, Y., Takayanagi, Y., Kinou, M., Araki, T., Harima, H., Fukuda, M., Okazaki, Y., Kasai, K., 2011. Different hemodynamic response patterns in the prefrontal cortical sub-regions according to the clinical stages of psychosis. Schizophr. Res. 132, 54–61.
Koutsouleris, N., Meisenzahl, E.M., Davatzikos, C., Bottlender, R., Frodl, T., Scheuerecker, J., Schmitt, G., Zetzsche, T., Decker, P., Reiser, M., Moller, H.J., Gaser, C., 2009. Use of neuroanatomical pattern classification to identify subjects in at-risk mental states of psychosis and predict disease transition. Arch. Gen. Psychiatry 66, 700–712.
Mathers, C.D., Loncar, D., 2006. Projections of global mortality and burden of disease from 2002 to 2030. PLoS Med. 3, e442.
McGorry, P.D., Killackey, E., Yung, A., 2008. Early intervention in psychosis: concepts, evidence and future directions. World Psychiatry 7, 148–156.
Obrig, H., Villringer, A., 2003. Beyond the visible—imaging the human brain with light. J. Cereb. Blood Flow Metab. 23, 1–18.
Okada, E., Delpy, D.T., 2003. Near-infrared light propagation in an adult head model. II. Effect of superficial tissue thickness on the sensitivity of the near-infrared spectroscopy signal. Appl. Opt. 42, 2915–2922.
Phillips, M.L., Vieta, E., 2007. Identifying functional neuroimaging biomarkers of bipolar disorder: toward DSM-V. Schizophr. Bull. 33, 893–904.
Prince, M., Patel, V., Saxena, S., Maj, M., Maselko, J., Phillips, M.R., Rahman, A., 2007. No health without mental health. Lancet 370, 859–877.
Schecklmann, M., Ehlis, A.C., Plichta, M.M., Fallgatter, A.J., 2008. Functional near-infrared spectroscopy: a long-term reliable tool for measuring brain activity during verbal fluency. Neuroimage 43 (1), 147–155.
Shattuck, D.W., Mirza, M., Adisetiyo, V., Hojatkashani, C., Salamon, G., Narr, K.L., Poldrack, R.A., Bilder, R.M., Toga, A.W., 2008. Construction of a 3D probabilistic atlas of human cortical structures. NeuroImage 39, 1064–1080.
Strangman, G., Boas, D.A., Sutton, J.P., 2002a. Non-invasive neuroimaging using near-infrared light. Biol. Psychiatry 52, 679–693.
Strangman, G., Culver, J.P., Thompson, J.H., Boas, D.A., 2002b. A quantitative comparison of simultaneous BOLD fMRI and NIRS recordings during functional brain activation. NeuroImage 17, 719–731.
Suto, T., Fukuda, M., Ito, M., Uehara, T., Mikuni, M., 2004. Multichannel near-infrared spectroscopy in depression and schizophrenia: cognitive brain activation study. Biol. Psychiatry 55, 501–511.
Takizawa, R., Kasai, K., Kawakubo, Y., Marumo, K., Kawasaki, S., Yamasue, H., Fukuda, M., 2008. Reduced frontopolar activation during verbal fluency task in schizophrenia: a multi-channel near-infrared spectroscopy study. Schizophr. Res. 99, 250–262.
Tsuzuki, D., Jurcak, V., Singh, A.K., Okamoto, M., Watanabe, E., Dan, I., 2007. Virtual spatial registration of stand-alone fNIRS data to MNI space. NeuroImage 34, 1506–1518.
Yamashita, Y., Maki, A., Ito, Y., Watanabe, E., Koizumi, H., 1996. Noninvasive near-infrared topography of human brain activity using intensity modulation spectroscopy. Opt. Eng. 35, 1046–1049.
Young, R.C., Biggs, J.T., Ziegler, V.E., Meyer, D.A., 1978. A rating scale for mania: reliability, validity and sensitivity. Br. J. Psychiatry 133, 429–435.
Zanelli, J., Reichenberg, A., Morgan, K., Fearon, P., Kravariti, E., Dazzan, P., Morgan, C., Zanelli, C., Demjaha, A., Jones, P.B., Doody, G.A., Kapur, S., Murray, R.M., 2010. Specific and generalized neuropsychological deficits: a comparison of patients with various first-episode psychosis presentations. Am. J. Psychiatry 167, 78–85.
Zimmermann, P., Bruckl, T., Nocon, A., Pfister, H., Lieb, R., Wittchen, H.U., Holsboer, F., Angst, J., 2009. Heterogeneity of DSM-IV major depressive disorder as a consequence of subthreshold bipolarity. Arch. Gen. Psychiatry 66, 1341–1352.

NeuroImage 109 (2015) 530

Contents lists available at ScienceDirect

NeuroImage

journal homepage: www.elsevier.com/locate/ynimg

Corrigendum

Corrigendum to "Neuroimaging-aided differential diagnosis of the depressive state" [Neuroimage 85: 498–507, 2014]

Ryu Takizawa, Masato Fukuda, Shingo Kawasaki, Kiyoto Kasai, Masaru Mimura, Shenhong Pu, Takamasa Noda, Shin-ichi Niwa, Yuji Okazaki on behalf of the Joint Project of Psychiatric Application of Near-Infrared Spectroscopy (JPSY-NIRS) Group

The authors have recently noticed errors as specified below. We sincerely apologize for not being able to notice them before publication, but confirmed that they did not affect any other parts of the study including sample sizes, data analyses, and statistical conclusions.

Corrigendum:

(1) Page 499

Error: The participants were recruited from *June* 2004 to June 2009, with the exception of recruitment at the initial site (Gunma University Hospital in Maebashi City), which was conducted over 6 years (*March* 2003 to *March* 2009).

Correction: The participants were recruited from *April* 2004 to June 2009, with the exception of recruitment at the initial site (Gunma University Hospital in Maebashi City), which was conducted over 6 years (*October* 2003 to *September* 2009).

Comment: We really apologize for the mistakes. However, they did not affect any data or data analysis at all.

(2) Page 500 & Flow diagram (page 506):

Error: (page 506) *Because our clinically valuable target were help-seeking unremitted patients, subsequently we excluded study participants with extremely mild symptoms* (HAMD score ≤ 5, *PANSS depression item score ≤ 1*, PANSS negative symptom score ≤ 11, PANSS general psychopathology score ≤ 21, or *PANSS positive symptom score–negative symptom score ≤ 11; the latter 3 criteria were based on the criteria from the PANSS manual for the 5th percentile of patients with mild SZ*, Kay et al., 1991).

Flow diagram (page 506): "Excluded extremely mild symptomatic patients"

Correct: [a)]*Our clinically valuable target were help-seeking unremitted patients. Moreover, clinicians do not necessarily rely on an objective biomarker for diagnosis of schizophrenia if clinical manifestation of a help-seeker is characterized by predominant positive symptoms relative to negative symptoms. Subsequently, we excluded study participants with*: HAMD score ≤ 5, [b)]PANSS negative symptom score ≤ 11, PANSS general psychopathology score ≤ 21, or PANSS positive symptom score–negative symptom score [c)]*≥12*; the latter 3 criteria were based on [d)]*the 5th percentile rank converted from raw scores among N = 138 schizophrenia patients from the PANSS rating manual (Kay et al., 1991).*

Flow diagram (page 506): *"Excluded extremely mild symptomatic patients and schizophrenia patients with extreme predominance with positive than negative symptoms"*

Comments:

[a)c)]The criterion of "PANSS positive symptom score–negative symptom score (composite score) ≤ 11" was an inclusion criterion which should be corrected to exclusion criterion of "≥12". Also, this exclusion criterion does not necessarily indicate exclusion of schizophrenia patients with extremely mild symptoms, but more precisely, exclusion of those with extreme predominance with positive than negative symptoms. Thus, we now state more precisely. Accordingly, the statement of "Excluded extremely mild symptomatic patients" in Flow diagram (page 506) should also be modified. These changes did not affect any data or data analysis at all.

[b)]"PANSS depression item score ≤ 1" was not used as a criterion. Thus, this was removed. Again, this is just a mistake in the text and did not affect data or data analysis at all.

[d)]Because there are various versions of tables presenting conversion of raw scores of the PANSS to percentile ranks (for example, in the original paper (Kay et al., Schizophrenia Bulletin, 1987), the sample size was N = 101), we wanted to clarify the source of information.

(3) Page 501:

Error: *LBPA40*

Correct: *LPBA40*

Again, the authors really regret these mistakes and sincerely apologize for potential confusions to readers.

DOI of original article: http://dx.doi.org/10.1016/j.neuroimage.2013.05.126.

http://dx.doi.org/10.1016/j.neuroimage.2015.01.021

Int J CARS (2015) 10:383–392
DOI 10.1007/s11548-014-1129-2

ORIGINAL ARTICLE

Diffusion tensor tractography of normal facial and vestibulocochlear nerves

Masanori Yoshino · Taichi Kin · Akihiro Ito · Toki Saito · Daichi Nakagawa · Kyousuke Kamada · Harushi Mori · Akira Kunimatsu · Hirofumi Nakatomi · Hiroshi Oyama · Nobuhito Saito

Received: 5 July 2014 / Accepted: 3 November 2014 / Published online: 20 November 2014

Abstract
Purpose Diffusion tensor tractography (DTT) is not adequately reliable for prediction of facial and vestibulocochlear (VII–VIII) nerve locations, especially relative to a vestibular schwannoma (VS). Furthermore, it is often not possible to visualize normal VII–VIII nerves by DTT (visualization rates were 12.5–63.6 %). Therefore, DTT post-processing was optimized for normal VII–VIII nerve visualization with and without manual noise elimination.
Methods DTT examinations of ten patients were evaluated to assess the improvement in performance by modifying seed region of interest (ROI) and fractional anisotropy (FA) threshold. Seed ROI was placed at the porus of the internal auditory meatus, and FA threshold values were either fixed or variable for each patient. DTT visualization of cranial nerves VII–VIII was evaluated and the noise effect was measured.
Results Cranial nerves VII–VIII were visualized in 90 % of patients without using manual noise elimination by modifying the seed ROI and FA threshold. The visualization rate with FA threshold of the upper limit in each patient (100 %) was significantly higher than that with FA threshold of 0.1 (75 %) ($p = 0.02$). The incidence rate of noise with FA threshold of the upper limit (10 %) was not significantly different than the FA threshold of 0.1 (20 %) ($p = 0.66$).
Conclusion Seed ROI modification and FA thresholding can improve the visualization of cranial nerve VII–VIII locations in DTT. This technique is promising for its potential to determine the relationship of cranial nerves VII–VIII to VS.

Keywords Diffusion tensor tractography · Facial nerve · Vestibulocochlear nerve · Seed region of interest · Fractional anisotropy threshold

Introduction

Diffusion tensor tractography (DTT) is one method that depicts diffusion tensor data and visualizes consecutive nerve fibers by tracking the direction of the diffusion tensor's maximum eigenvalue λ_1 with arbitrary seed regions of interests (ROIs) [1]. DTT is dependent on the conditions of diffusion tensor imaging, such as slice thickness or pixel size, as well as fiber tracking condition settings such as the seed ROI, end point, fractional anisotropy (FA) threshold, turning angle, and step length of fiber tracking [2–7]; therefore, reliability becomes an issue since the results greatly vary by modifying each of these conditions. Consequently, with the objective to improve reliability of white matter fiber visualization, numerous studies to determine optimal conditions for diffusion tensor imaging and fiber tracking have been conducted [4–17]. As a result, DTT has been widely used to visualize white matter fibers [2,4,11,13,14]. Through recent

M. Yoshino (✉) · T. Kin · A. Ito · D. Nakagawa · H. Nakatomi · N. Saito
Department of Neurosurgery, Graduate School of Medicine, The University of Tokyo, 7-3-1 Hongo, Bunkyo-ku, Tokyo 113-8655, Japan
e-mail: ymasa-tky@umin.ac.jp

T. Saito · H. Oyama
Department of Clinical Information Engineering, Graduate School of Medicine, The University of Tokyo, 7-3-1 Hongo, Bunkyo-ku, Tokyo 113-8655, Japan

K. Kamada
Department of Neurosurgery, Asahikawa Medical University, 2-1, Midorigaoka-Higashi, Asahikawa, Hokkaido 078-8510, Japan

H. Mori · A. Kunimatsu
Department of Radiology, Graduate School of Medicine, The University of Tokyo, 7-3-1 Hongo, Bunkyo-ku, Tokyo 113-8655, Japan

studies, it has been discovered that not only intracerebral white matter fibers, but also cranial and peripheral nerves, can be visualized [18–23]. Moreover, it has been reported that the visualization of the facial nerve that is elongated by vestibular schwannoma (VS), which used to be problematic with traditional morphological imaging alone, is feasible with this technique [18,24–26]. However, condition settings for diffusion tensor imaging and fiber tracking in patients with VS vary greatly among studies [18,24–26]; thus, appropriate settings have not been established. More importantly, the method to distinguish the facial and vestibulocochlear (VII–VIII) nerve from surrounding noise has not been established for fiber tracking in patients with VS. Therefore, it is hard to assess whether visualized fibers truly represent the nerve. In addition, it was not possible to constantly visualize normal facial and vestibulocochlear nerves with DTT according to previous reports (visualization rates were 12.5–63.6 %) [18,19,21]. Based on the above-mentioned information, it appears that the current DTT is not entirely reliable when using DTT to predict the facial and vestibulocochlear nerve location in relation to the VS. Therefore, keeping in mind the objective of the present study to help increase the reliability of DTT enough to use it daily in the prediction of facial and vestibulocochlear nerves location in relation to VS, we investigated the DTT conditions for normal facial and vestibulocochlear nerves. Our aim was to improve both its visualization performance and establish a way to distinguish facial and vestibulocochlear nerves from the surrounding noises without using manual elimination based on the anatomical knowledge. In addition, diffusion tensor imaging conditions and fiber tracking conditions need to be studied [2,6]; however, imaging conditions vary greatly depending on the instrument used. Therefore, the present study assessed the fiber tracking condition settings. Furthermore, since it is currently difficult to constantly and separately visualize facial and vestibulocochlear nerves with DTT [21], we evaluated the visualization performance of both nerves together and subsequently referred to this visualization target as the VII–VIII nerve complex.

Methods

Patient population

We investigated 10 patients {5 men and 5 women, mean age of 61 years (standard deviation = 11.5 years)} with supratentorial aneurysms who were admitted to the Department of Neurosurgery at the University of Tokyo hospital for treatment. These patients have never exhibited hearing impairment or facial disorders, and diffusion tensor image and fast imaging employing steady state acquisition (FIESTA) were taken as preoperative tests.

The internal review board at the University of Tokyo Hospital approved the study protocol, and written informed consent was obtained from all subjects prior to participation.

Image acquisition

MRI was performed using a 3.0-T system (Signa 3.0T; GE, Wisc., USA) equipped with an 8-channel phased-array head coil. DT images were obtained with a single-shot spin-echo echo-planar sequence using the following protocol: response time (TR), 17,000 ms; echo time, 65.6 ms; slice thickness, 2.5 mm with no gap; field of view (FOV), 25.6 cm; number of excitations, 1; matrix size, 128 × 128; reconstructed images were zero-fill interpolated to 256 × 256. DT imaging data were acquired along 30 non-collinear gradient directions with a b value of 1,000 s/mm^2 and an additional zero b-image (B0 image). Realignment of these images and compensation for eddy-current morphing were performed, using a mutual-information-based algorithm [27] on a workstation equipped with the MR unit (Functool2; GE, Milwaukee, WI, USA). We also acquired anatomical MR images using a FIESTA with following protocol: TR, 4.2 ms; TE, 1.6 ms; slice thickness, 0.4 mm; FOV, 20 cm; matrix size, 512 × 512; flip angle, 45°; voxel size, 0.39 × 0.39 × 0.4 mm; and slice number, 228.

DTI and FIESTA data were transferred to a personal computer (Precision T7500; Dell, Round Rock, TX; CPU: Intel Xeon X5550, 2.67 GHz, 2.66 GHz; PAM: 8.00 GB; graphics card: NVIDIA Quadro FX5800). DTT was performed using volume-one 1.72 and dTV-II SR [3] that utilize deterministic tractography procedure, a single-tensor approach and maximum path lengths set. Regions of interest (ROI) and FA thresholds are described in the next section. Target ROI was not used. As for other parameters, such as step length and turning angle, we used a default value of dTV (step length; 160, turning angle; 30°). Interpolation along the z axis was applied to obtain isotropic data (with a voxel size of 0.9 × 0.9 × 0.9). We also used Avizo 6.3 software (Visualization Science Group, Bordeaux, France) for co-registration between DTT and FIESTA, and then used rigid registration with normalized mutual information as a value for co-registration between them.

Fiber tracking condition setting of proposed method

Of the fiber tracking conditions, seed ROI and FA threshold for fiber tracking are known to greatly influence the fiber tracking results [2,6]. Specifically, seed ROI refers to the position where fiber tracking calculations are initiated within the image, and if an incorrect position is selected, fibers other than the target fibers are visualized; thus, it is important to select an appropriate seed ROI. However, previous reports often only explained that "[seeds] were placed at the internal auditory meatus," regarding the seed ROI placement in

DTT of normal facial nerve, vestibulocochlear nerve, and vestibular schwannoma [21,24,25]. Moreover, other reports differed in their methodology [18,19,26], and the assessment of seed ROI placement methods was not adequate. In addition, FA threshold is one of the parameters used during fiber tracking, and if FA value of the target tissue is lower than the FA threshold value that has been set, fiber tracking is completed. In other words, if FA threshold is set low, the detection of noise from non-neural tissues increases. Conversely, although noise decreases if FA threshold is maintained at a higher level, the target nerve for visualization could also disappear if this level is inappropriately high [4,6,17]. For these reasons, it is also important to set the FA threshold at an appropriate value; however, optimal conditions have not been previously investigated, and in many cases, the threshold values were arbitrary selected between 0.1 and 0.2 [18,19,21,24–26]. Therefore, in the present study, with considerations for problems with existing methods, we used the following methods (a) and (b) to establish seed ROI and FA thresholds (Fig. 1).

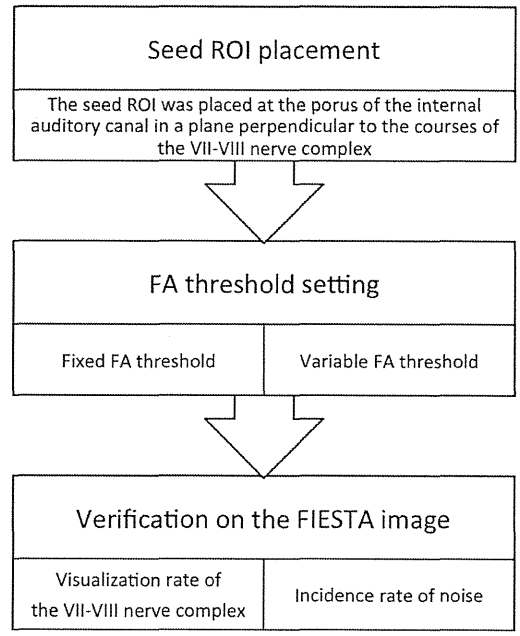

Fig. 1 Flowchart of this study. First, we set the region of interest (ROI) at the porus of the internal auditory meatus in a plane perpendicular to the courses of the VII–VIII nerve complex. Next, we performed the fiber tracking either with fixed fractional anisotropy (FA) threshold values or with variable FA threshold values. Finally, we displayed the visualized fibers after aligning them to fast imaging employing steady state acquisition (FIESTA), and assessed the DTT visualization performance of the VII–VIII nerve complex by using the visualization rate of the VII–VIII nerve complex and the incidence rate of noise in each FA threshold value setting. In this case, visualization rate was calculated as the percentage of patients with fibers corresponding to VII–VIII nerve complex on FIESTA of all patients. Incidence rate of noise was calculated as the percentage of patients with fibers corresponding with noise of the total number of patients

Seed ROI placement

The facial nerve, cochlear nerve, and vestibular nerve that rotate three-dimensionally and pass through the internal auditory meatus [28–30] were all included in the seed ROI, and in order to eliminate the effect of the planar structure of the fundus of the internal auditory meatus on tensor analysis, we proposed a method to "select the internal auditory meatus on a plane perpendicular to the facial and vestibulocochlear nerves passing through at the porus of the internal auditory meatus." Detailed methods are shown in Fig. 2. We first viewed the opening to the internal auditory meatus from a direction parallel to the nerve passing through the internal auditory meatus (Fig. 2a, arrowhead), and placed the seed ROI at the porus of the internal auditory canal in a plane perpendicular to the courses of the VII–VIII nerve complex. In addition, when placing the seed ROI, the internal auditory meatus was encircled with a manually created line for each individual patient such that surrounding tissues were included as little as possible (Fig. 2b, circle). All of these procedures were conducted on the B0 image; however, if confirming the internal auditory meatus was deemed difficult, a distribution map of appropriate apparent diffusion coefficients (ADC) (ADC map) was used.

FA threshold setting

Since the measured FA value may decrease depending on the partial volume effect for facial and vestibulocochlear nerves, we added 0.00, 0.05 in addition to values from previous reports (0.1–0.2) and set the FA thresholds at 0.00, 0.05, 0.10, 0.15, and 0.20. In addition, since there is individual variation in the development of mastoid cells [31], individual variation in the effects of signal degradation caused by magnetic susceptibility artifacts is also suspected in the facial and vestibulocochlear nerves. Therefore, we also set variable threshold values per each individual. Specifically, for each patient, we increased the FA threshold by 0.01 from 0.00 and determined the FA threshold value immediately before the fiber disappeared. We then set this FA threshold as the upper limit and subsequently set FA thresholds at the upper limit and at 75, 50, 25, and 0 % for each individual patient (Fig. 1). For the remainder of this manuscript, the former will be referred to as fixed FA threshold value setting and the latter will be referred to as variable FA threshold value setting.

Verification of the visualized fiber and assessment of appropriate FA threshold of the proposed method

With the VII–VIII nerve complex confirmed on the FIESTA image as "true," we verified the fiber and assessed the DTT

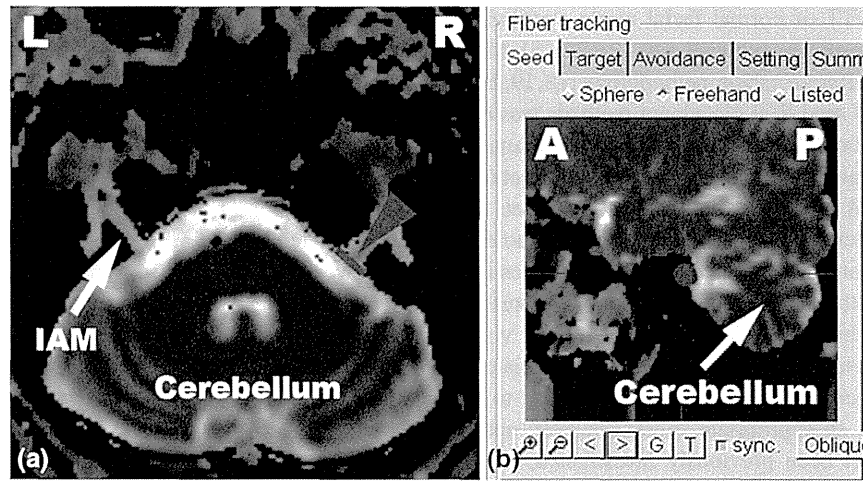

Fig. 2 Seed region of interest (ROI) placement method. The porus of the internal auditory meatus was viewed from a direction parallel to the nerve that passes through the internal auditory meatus (**a** *red arrowhead*), and the seed ROI was placed on a plane that is perpendicular to the nerve passing through at the porus of the internal auditory meatus (**b** *red circle*). *IAM* internal auditory meatus, *L* left, *R* right, *A* anterior, *P* posterior

visualization performance of the VII–VIII nerve complex. First, we displayed the visualized fibers after aligning them to FIESTA [32] and then classified fibers that pass through VII–VIII nerve complex on FIESTA as VII–VIII nerve complex, and fibers that pass through all other areas as noise. Subsequently, we evaluated the visualization rate of VII–VIII nerve complex and the incidence rate of noise in the fixed FA threshold value setting. In this case, visualization rate was calculated as the percentage of patients with fibers corresponding with VII–VIII nerve complex on FIESTA out of all patients. Incidence rate of noise was calculated as the percentage of patients with fibers corresponding with noise of the total number of patients (Fig. 1). We then decided the FA threshold, with which both the visualization rate of VII–VIII nerve complex was high and incidence rate of noise was low, to be the appropriate FA threshold since the aim of this study was to propose the setting that enabled us to visualize only the VII–VIII nerve complex constantly without using manual elimination of noise based on anatomical knowledge. Subsequently, the appropriate FA threshold in the variable FA threshold value setting was evaluated in a similar manner. Finally, when comparing visualization and incidence rates of appropriate FA threshold in the fixed FA threshold value setting with that of appropriate FA threshold in the variable FA threshold value setting, we decided the FA threshold, with which visualization rate was higher and incidence rate was lower, to be the appropriate FA threshold for our methodology.

DTT visualization was performed by one neurosurgeon (M.Y.), and verification after alignment was conducted by consulting with a neurosurgeon who was not involved in DTT visualization (T.K.). The above-mentioned neurosurgeons were neurosurgery specialists.

Statistical analysis

Chi-square test was used for comparison of the visualization rates of VII–VIII nerve complex and the appearance rates of noise. Statistical analyses were conducted using SPSS for Mac Version 21 (SPSS Inc, IBM, Somers, NY).

Results

Verification of the visualized fiber and assessment of appropriate FA threshold of proposed method

First, we verified the visualized fiber on FIESTA with fixed FA threshold value setting and found that the number of patients with fibers classified as a VII–VIII nerve complex was the highest (10 out of 10 patients) with FA thresholds of 0.00 and 0.05, and the number of patients with fibers classified as a VII–VIII nerve complex decreased with the increase in FA threshold values (8 out of 10, 1 out of 10, and 0 out of 10 with FA thresholds of 0.10, 0.15, and 0.20, respectively). Similarly, the number of patients with fibers classified as noise was the highest (10 out of 10 patients) with FA thresholds of 0.00 and 0.05, and decreased with the increase in FA threshold values (4 out of 10, 1 out of 10, and 0 out of 10 with FA thresholds of 0.10, 0.15, and 0.20, respectively) (Table 1). We investigated this threshold value setting with the visualization rate of the VII–VIII nerve complex and the incidence rate of noise, and found that the visualization rate of VII–VIII nerve complex was the highest (100 %) with FA threshold of 0.00 and 0.05, but the incidence rate of noise was also high (95–100 %) with these thresholds. In contrast, the incidence rate of noise was the lowest (0 %) with FA threshold

Table 1 Verification results of fibers visualized with fixed fractional anisotropy (FA) threshold values

Test subject	FA threshold: 0.00	FA threshold: 0.05	FA threshold: 0.10	FA threshold: 0.15	FA threshold: 0.20
1R	①, ②	①, ②	–	–	–
1L	①, ②	①, ②	①	–	–
2R	①, ②	①, ②	①, ②	–	–
2L	①, ②	①, ②	①	–	–
3R	①, ②	①	–	–	–
3L	①, ②	①, ②	–	–	–
4R	①, ②	①, ②	①	–	–
4L	①, ②	①, ②	①	–	–
5R	①, ②	①, ②	–	–	–
5L	①, ②	①, ②	–	–	–
6R	①, ②	①, ②	①	–	–
6L	①, ②	①, ②	①	–	–
7R	①, ②	①, ②	①, ②	–	–
7L	①, ②	①, ②	①	–	–
8R	①, ②	①, ②	①	–	–
8L	①, ②	①, ②	①, ②	–	–
9R	①, ②	①, ②	①	–	–
9L	①, ②	①, ②	①, ②	①	–
10R	①, ②	①, ②	①	–	–
10L	①, ②	①, ②	①	–	–

① Fibers that pass through facial and vestibulocochlear (VII–VIII) nerve complex on fast imaging employing steady state acquisition (FIESTA)
② Fibers that did not pass through VII–VIII nerve complex on FIESTA
– Not visualized

of 0.15 and 0.20, but the visualization rate of VII–VIII nerve complex at these thresholds was also low (0–5 %). Finally, we found that the visualization rate of VII–VIII nerve complex was high (75 %) and the incidence rate of noise was low (20 %) with FA threshold of 0.10, and decided FA threshold of 0.10 as the appropriate setting in the fixed FA threshold value setting (Fig. 3a).

Next, with variable FA threshold value setting, the number of patients with fibers classified as noise was the highest (10 out of 10 patients) with FA thresholds of 0.00, 0.05, and 0.10, and decreased with the increase in FA threshold (8 out of 10 and 2 out of 10 with FA thresholds of 0.15 and 0.20, respectively). In contrast, fibers classified as VII–VIII nerve complex could be confirmed in all patients at all FA threshold values (Table 2). We also found that the visualization rate was consistently 100 % regardless of the FA threshold, and that the incidence rate of noise decreased with FA threshold increase, and was the lowest (10 %) when the FA threshold was set at the upper limit (Fig. 3b). Therefore, we decided the upper limit to be an appropriate setting in the variable FA threshold value setting.

We then compared visualization and incidence rates with appropriate FA threshold in each setting and found that the visualization rate of VII–VIII with FA threshold of the upper limit was significantly higher than that with FA threshold of 0.1 ($\chi^2_{1df} = 7.059$, $p = 0.02$), and the incidence rate of noise with FA threshold of the upper limit was lower than that with FA threshold of 0.1 ($\chi^2_{1df} = 0.784$, $p = 0.66$). As a result, FA threshold of the upper limit was considered the appropriate FA threshold of our methodology. FA threshold values of the upper limit in each patient were 0.10 ± 0.04 (mean $\pm$ standard deviation) (Table 3).

Representative case presentation

Case: 8R

We performed a visualization using fixed FA threshold values (Fig. 4) and found that fibers that correspond with the right VII–VIII nerve complex could be visualized with fixed FA threshold values of 0.00, 0.05, and 0.10. However, because noises appeared at the same time, we were not able to visualize just the fibers that correspond with the right VII–VIII nerve complex. Additionally, these fibers were not visualized with FA threshold values beyond 0.15.

In contrast, fibers that correspond with the VII–VIII nerve complex were visualized with any of the variable FA threshold values (Fig. 5). Also, noises appeared with FA threshold values up to 75 % of the upper limit; however, only fibers that correspond with the VII–VIII nerve complex could be

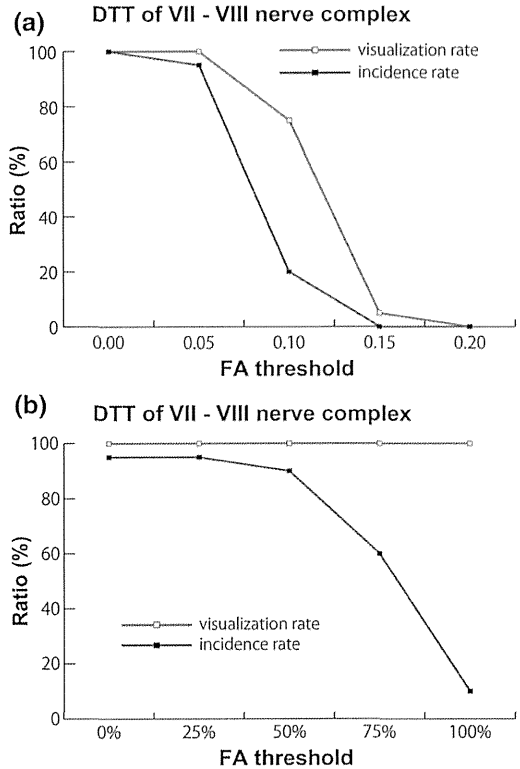

Fig. 3 **a** Visualization and incidence rates with fixed fractional anisotropy (FA) threshold values. **b** Visualization and incidence rates with variable FA threshold values. Visualization rate was calculated as the percentage of patients with fibers corresponding with the facial and vestibulocochlear nerve complex on FIESTA. Incidence rate of noise was calculated as the percentage of patients with fibers corresponding with noise

Table 2 Verification results of fibers visualized with variable fixed fractional anisotropy (FA) threshold values

Test subject	FA threshold: 0 %	FA threshold: 25 %	FA threshold: 50 %	FA threshold: 75 %	FA threshold: upper limit
1R	①, ②	①, ②	①, ②	①, ②	①
1L	①, ②	①, ②	①, ②	①	①
2R	①, ②	①, ②	①, ②	①, ②	①
2L	①, ②	①, ②	①, ②	①	①
3R	①	①	①	①	①
3L	①, ②	①, ②	①, ②	①, ②	①, ②
4R	①, ②	①, ②	①, ②	①	①
4L	①, ②	①, ②	①, ②	①	①
5R	①, ②	①, ②	①, ②	①, ②	①, ②
5L	①, ②	①, ②	①, ②	①, ②	①
6R	①, ②	①, ②	①, ②	①	①
6L	①, ②	①, ②	①	①	①
7R	①, ②	①, ②	①, ②	①, ②	①
7L	①, ②	①, ②	①, ②	①, ②	①
8R	①, ②	①, ②	①, ②	①, ②	①
8L	①, ②	①, ②	①, ②	①, ②	①
9R	①, ②	①, ②	①, ②	①, ②	①
9L	①, ②	①, ②	①, ②	①, ②	①
10R	①, ②	①, ②	①, ②	①, ②	①
10L	①, ②	①, ②	①, ②	①, ②	①

① Fibers that pass through facial and vestibulocochlear (VII–VIII) nerve complex on fast imaging employing steady state acquisition (FIESTA)
② Fibers that did not pass through VII–VIII nerve complex on FIESTA – Not visualized

visualized when the FA threshold was set at the upper limit (Fig. 5).

Discussion

In the present study, we were able to increase the visualization rate of VII–VIII nerve complex and decrease the incidence rate of noise by investigating fiber tracking conditions, such as seed ROI placement method and FA threshold setting method, without using manual elimination based on the anatomical knowledge.

Fiber tracking conditions for normal facial and vestibulocochlear nerves

Seed ROI

In order to assess the influence of seed ROI setting on visualization rate, we compared visualization rate of our result with that of Kabasawa et al. [19] (seed ROI placement to the internal auditory meatus on the axial cross section; FA threshold: 0.1) and Taoka et al. [18] (seed ROI placement to the fundus of internal auditory meatus on the sagittal cross section; FA threshold: 0.1). In this comparison, our result with the FA threshold of 0.1 was used because FA threshold in these two reports was also 0.1. As a result, we found that our result of visualization with FA threshold of 0.1 was 75 %. On the other hand, results of the two above-mentioned reports were 37.5 and 12.5 %, respectively. Although it is difficult to compare these results simply because each diffusion tensor imaging condition was different, we found that our visualization rate was much higher than that of the previous reports. Therefore, it is speculated that the reason why the visualization rate was higher with our setting even with the same FA threshold conditions, was due to the fact that all nerves that passed through the internal auditory meatus could be included in the seed ROI, which is placed on a plane perpendicular to the nerve passing through. On the other hand, it is difficult to entirely include the nerve with the seed ROI described by Kabasawa et al. [19]. We, therefore, speculated that this led to the decrease in visualization rate. Moreover,

Table 3 Fractional anisotropy threshold values of the upper limit in each patient

Test subject	FA threshold value: upper limit
1R	0.07
1L	0.11
2R	0.08
2L	0.12
3R	0.09
3L	0.08
4R	0.06
4L	0.06
5R	0.08
5L	0.08
6R	0.1
6L	0.2
7R	0.13
7L	0.08
8R	0.1
8L	0.13
9R	0.1
9L	0.18
10R	0.11
10L	0.12

just as the visualization rate was low with the seed ROI as described by Taoka et al. [18], it is speculated that the fundus of the internal auditory meatus was more susceptible to signal degradation caused by magnetic susceptibility artifacts compared to the opening to the internal auditory meatus. In addition, when eigenvalue analysis is performed at the site where nerve fibers intersect, $\lambda_1 \gg \lambda_2 \fallingdotseq \lambda_3$ is not necessarily true, and the FA value is known to decrease [6,33]. At the fundus of the internal auditory meatus, since the nerve fiber and the bone of the fundus of internal auditory meatus are orthogonal to each other, eigenvalue analysis at this same site is affected for a similar reason and FA value is decreased. It is speculated that this influenced the DTT visualization rate.

FA threshold

The optimal FA threshold for pyramidal tract during DTT is reported to be approximately 0.2 [4]. In this study, FA threshold values of the upper limit in each patient were 0.10 ± 0.04 (mean $\pm$ standard deviation); therefore, a FA threshold value of 0.1, which was used in several studies, seemed reasonable. However, the present results suggested that setting the FA threshold based on the upper limits

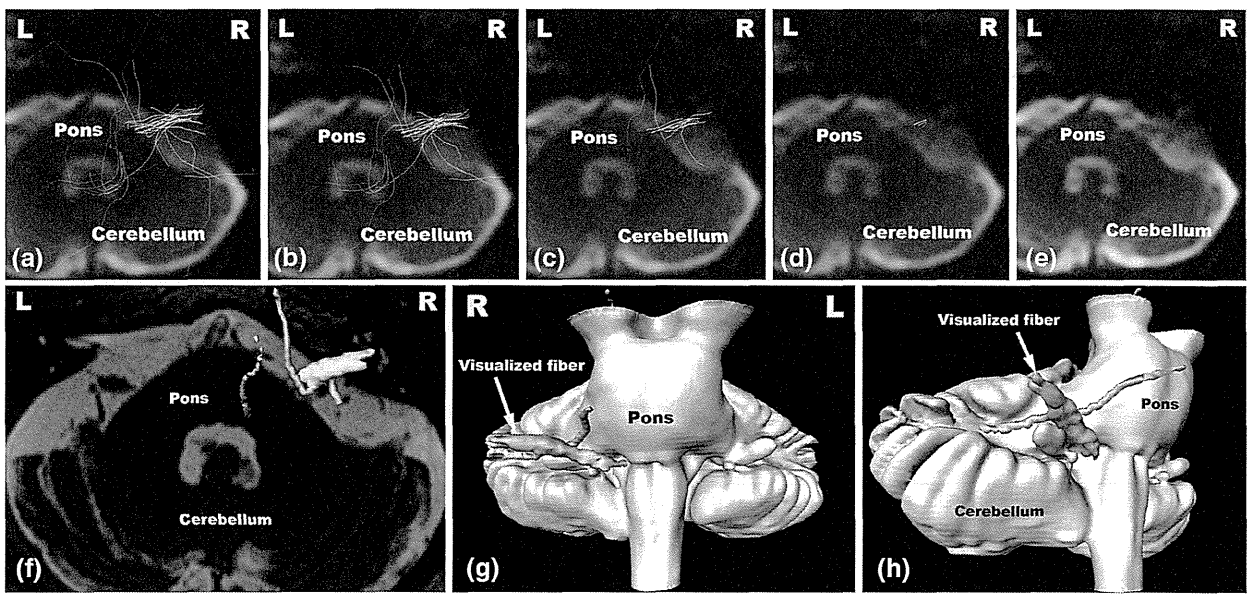

Fig. 4 Verification with diffusion tensor tractography (DTT) and fast imaging employing steady state acquisition (FIESTA) using fixed fractional anisotropy (FA) threshold values (**a–e** axial cross section of the B0 image, **f** axial cross section of FIESTA, **g** anterior to posterior view of a three-dimensional anatomical image, **h** oblique view of a three-dimensional anatomical image. FA threshold of **a** 0.00, **b** 0.05, **c** 0.10, **d**: 0.15, and **e** 0.20. **f** Fibers visualized at FA threshold of 0.10 were voxelized and depicted on FIESTA. **g**, **h** Fibers visualized at FA threshold of 0.10 were voxelized and depicted on three-dimensional anatomical image). Although fibers that did not correspond with facial and vestibulocochlear (VII–VIII) nerve complex decreased by increasing the FA threshold, it was difficult to visualize only fibers that corresponded with VII–VIII nerve complex at any FA threshold. *L* left, *R* right

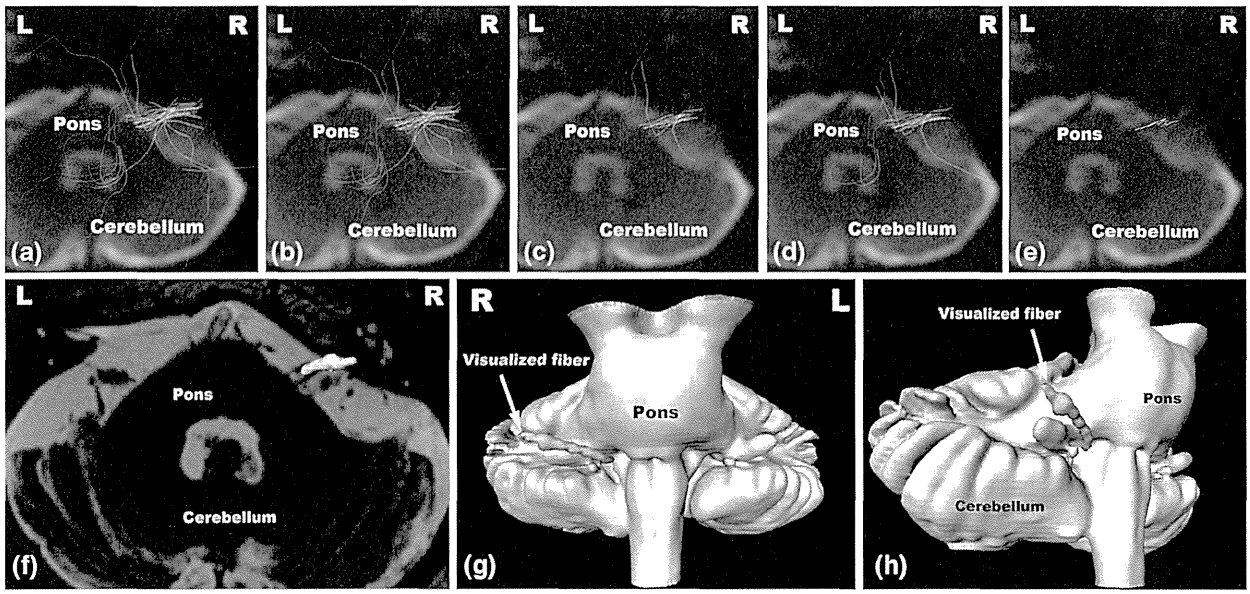

Fig. 5 Verification with diffusion tensor tractography (DTT) and fast imaging employing steady state acquisition (FIESTA) using variable fractional anisotropy (FA) threshold values (**a–e** axial cross section of the B0 image, **f** axial cross section of FIESTA, **g**: anterior to posterior view of a three-dimensional anatomical image, **h** oblique view of a three-dimensional anatomical image. **a** 0 %, **b** 25 %, **c** 50 %, **d** 75 %, and **e** 100 % (upper limit) of the FA threshold upper limit. **f** Fibers visualized at FA threshold of upper limit were voxelized and depicted on FIESTA. **g**, **h** fibers visualized at FA threshold of upper limit were voxelized and depicted on three-dimensional anatomical image). By increasing the FA threshold, fibers that did not correspond with facial and vestibulocochlear (VII–VIII) nerve complex decreased, and only fibers that corresponded with VII–VIII nerve complex, when FA threshold was set at the upper limit, could be visualized. *L* left, *R* right

Table 4 Comparison of proposed method with existing methods

Series	Software	FA threshold	Seed ROI	Visualization rate
Taoka et al. [18]	DTV	0.1	Placement at the fundus of the internal auditory meatus on the sagittal cross section	12.5 %
Kabasawa et al. [19]	DTV	0.1	Placement to the internal auditory meatus on the axial cross section	37.5 %
Hodaie et al. [21]	3D slicer	0.2	Placement to the internal auditory meatus	63.6 %
Roundy et al. [26]	Track Vis	0.15	Placement on the nerve passing through the middle of the cistern on sagittal cross section	Not described
Present study	DTV	Upper limit for each patient	Placement at the porus of the internal auditory meatus on a plane perpendicular to the facial and vestibulocochlear nerves	100 %

Visualization rate was calculated as the percentage of patients that could visualize the facial and vestibulocochlear nerves out of all patients

for each patient rather than with fixed values can improve visualization rate of VII–VIII nerve complex and decrease appearance rate of noise. The reason for this, compared to supratentorial structures such as the pyramidal tract, is that the area near internal auditory meatus is easily influenced by magnetic susceptibility artifacts caused by mastoid cells, etc. [6]. Therefore, it is speculated that the large individual differences by patient in the FA value of VII–VIII nerve complex contributed to this observation. From the above findings, we considered that, in DTT for normal facial and vestibulocochlear nerves, it is difficult to make adjustments for individual variation of each patient using fixed values, and it is therefore necessary to use variable values.

Comparison with existing reports

There are four existing reports regarding DTT of normal facial and vestibulocochlear nerves. We compared our study with these reports (Table 4). As mentioned, the seed ROI placement is considered to be one of the reasons for decreased visualization rate in the reports by Taoka et al. and Kabasawa et al. Additionally, in a report by Hodaie et al. [21], the placement method of seed ROI was only described as "internal auditory meatus"; thus, it was difficult to make comparisons because detailed method of setting the seed ROI was not mentioned. In a report by Roundy et al. [26], seed ROI was placed on the nerve that passes through the cistern. Their method reproducibility, however, seems low because there are often difficulties confirming normal facial and vestibulocochlear nerves with diffusion tensor imaging. Therefore, we excluded this report for the purposes of comparison. Furthermore, all of these reports used fixed FA threshold values, and it is postulated that this also contributed to the decrease in visualization rate.

Limitations

In the present study, we were able to both increase the visualization rate and decrease the incidence rate by modifying the methods for seed ROI placement and FA threshold setting. However, increasing the FA threshold and setting it at the upper limit not only reduces noise, but also decreases the target nerve to be visualized. For this reason, it is highly probable that fibers viewed at the upper limit visualize only a part of VII–VIII nerve complex. However, to achieve the ultimate goal, which is to improve the precision in predicting the facial and vestibulocochlear nerve locations in relation to vestibular schwannomas, a method to extract nerve fibers alone from the abundance of noise is necessary. We, therefore, postulate that the present method will prove useful.

Conclusion

In the present study, we were able to achieve both the visualization rate of the VII–VIII nerve complex of 100 % and incidence rate of noise of 10 %, by placing the seed ROI on a plane that is perpendicular to the nerve passing through the porus of the internal auditory meatus, and by setting the FA threshold at the upper limit for each patient. Since the present method enabled us to visualize only VII–VIII nerve complex in 90 % patients without using manual elimination of noise based on the anatomical knowledge, we considered this method to be a highly anticipated means to improve the prediction of the facial and vestibulocochlear nerve locations in relation to vestibular schwannomas.

Acknowledgments We would like to thank Minoru Tanaka for suggesting this investigation. This work was supported in part by a Grant-in-Aid for Challenging Exploratory Research (25670618).

Conflic of interest The authors report no conflict of interest concerning the materials or methods used in this study as well as the findings specified in this paper.

References

1. Mori S, Crain BJ, Chacko VP, van Zijl PC (1999) Three-dimensional tracking of axonal projections in the brain by magnetic resonance imaging. Ann Neurol 45(2):265–269
2. Mori S, van Zijl PC (2002) Fiber tracking: principles and strategies—a technical review. NMR Biomed 15(7–8):468–480. doi:10.1002/nbm.781
3. Masutani Y, Aoki S, Abe O, Hayashi N, Otomo K (2003) MR diffusion tensor imaging: recent advance and new techniques for diffusion tensor visualization. Eur J Radiol 46(1):53–66
4. Kunimatsu A, Aoki S, Masutani Y, Abe O, Hayashi N, Mori H, Masumoto T, Ohtomo K (2004) The optimal trackability threshold of fractional anisotropy for diffusion tensor tractography of the corticospinal tract. Magn Reson Med Sci 3(1):11–17
5. Jiang H, van Zijl PC, Kim J, Pearlson GD, Mori S (2006) DtiStudio: resource program for diffusion tensor computation and fiber bundle tracking. Comput Methods Programs Biomed 81(2):106–116. doi:10.1016/j.cmpb.2005.08.004
6. Mukherjee P, Chung SW, Berman JI, Hess CP, Henry RG (2008) Diffusion tensor MR imaging and fiber tractography: technical considerations. Am J Neuroradiol 29(5):843–852. doi:10.3174/ajnr.A1052
7. Akazawa K, Yamada K, Matsushima S, Goto M, Yuen S, Nishimura T (2010) Optimum b value for resolving crossing fibers: a study with standard clinical b value using 1.5-T MR. Neuroradiology 52(8):723–728. doi:10.1007/s00234-010-0670-0
8. Byrnes TJ, Barrick TR, Bell BA, Clark CA (2009) Semiautomatic tractography: motor pathway segmentation in patients with intracranial vascular malformations. Clinical article. J Neurosurg 111(1):132–140. doi:10.3171/2009.2.JNS08930
9. Lori NF, Akbudak E, Shimony JS, Cull TS, Snyder AZ, Guillory RK, Conturo TE (2002) Diffusion tensor fiber tracking of human brain connectivity: acquisition methods, reliability analysis and biological results. NMR Biomed 15(7–8):494–515. doi:10.1002/nbm.779
10. Tournier JD, Calamante F, King MD, Gadian DG, Connelly A (2002) Limitations and requirements of diffusion tensor fiber tracking: an assessment using simulations. Magn Reson Med 47(4):701–708
11. Clark CA, Barrick TR, Murphy MM, Bell BA (2003) White matter fiber tracking in patients with space-occupying lesions of the brain: a new technique for neurosurgical planning? Neuroimage 20(3):1601–1608
12. Jones DK (2004) The effect of gradient sampling schemes on measures derived from diffusion tensor MRI: a Monte Carlo study. Magn Reson Med 51(4):807–815. doi:10.1002/mrm.20033
13. Kamada K, Todo T, Masutani Y, Aoki S, Ino K, Takano T, Kirino T, Kawahara N, Morita A (2005) Combined use of tractography-integrated functional neuronavigation and direct fiber stimulation. J Neurosurg 102(4):664–672
14. Kamada K, Todo T, Morita A, Masutani Y, Aoki S, Ino K, Kawai K, Kirino T (2005) Functional monitoring for visual pathway using real-time visual evoked potentials and optic-radiation tractography. Neurosurgery 57(1):121

15. Okada T, Miki Y, Fushimi Y, Hanakawa T, Kanagaki M, Yamamoto A, Urayama S, Fukuyama H, Hiraoka M, Togashi K (2006) Diffusion-tensor fiber tractography: intraindividual comparison of 3.0-T and 1.5-T MR imaging1. Radiology 238(2):668–678
16. Nucifora PGP, Verma R, Lee SK, Melhem ER (2007) Diffusion-tensor MR imaging and tractography: exploring brain microstructure and connectivity1. Radiology 245(2):367–384
17. Stadlbauer A, Nimsky C, Buslei R, Salomonowitz E, Hammen T, Buchfelder M, Moser E, Ernst-Stecken A, Ganslandt O (2007) Diffusion tensor imaging and optimized fiber tracking in glioma patients: histopathologic evaluation of tumor-invaded white matter structures. Neuroimage 34(3):949–956. doi:10.1016/j.neuroimage.2006.08.051
18. Taoka T, Hirabayashi H, Nakagawa H, Sakamoto M, Myochin K, Hirohashi S, Iwasaki S, Sakaki T, Kichikawa K (2006) Displacement of the facial nerve course by vestibular schwannoma: preoperative visualization using diffusion tensor tractography. J Magn Reson Imaging 24(5):1005–1010. doi:10.1002/jmri.20725
19. Kabasawa H, Masutani Y, Aoki S, Abe O, Masumoto T, Hayashi N, Ohtomo K (2007) 3T PROPELLER diffusion tensor fiber tractography: a feasibility study for cranial nerve fiber tracking. Radiat Med 25(9):462–466. doi:10.1007/s11604-007-0169-8
20. Andreisek G, White LM, Kassner A, Tomlinson G, Sussman MS (2009) Diffusion tensor imaging and fiber tractography of the median nerve at 1.5T: optimization of b value. Skeletal Radiol 38(1):51–59. doi:10.1007/s00256-008-0577-6
21. Hodaie M, Quan J, Chen DQ (2010) In vivo visualization of cranial nerve pathways in humans using diffusion-based tractography. Neurosurgery 66(4):788–795. doi:10.1227/01.NEU.0000367613.09324.DA discussion 795–786
22. Hodaie M, Chen DQ, Quan J, Laperriere N (2012) Tractography delineates microstructural changes in the trigeminal nerve after focal radiosurgery for trigeminal neuralgia. PLoS One 7(3):e32745. doi:10.1371/journal.pone.0032745
23. Cauley KA, Filippi CG (2013) Diffusion-tensor imaging of small nerve bundles: cranial nerves, peripheral nerves, distal spinal cord, and lumbar nerve roots-clinical applications. AJR Am J Roentgenol 201(2):W326–335. doi:10.2214/AJR.12.9230
24. Chen DQ, Quan J, Guha A, Tymianski M, Mikulis D, Hodaie M (2011) Three-dimensional in vivo modeling of vestibular schwannomas and surrounding cranial nerves with diffusion imaging tractography. Neurosurgery 68(4):1077–1083. doi:10.1227/NEU.0b013e31820c6cbe
25. Gerganov VM, Giordano M, Samii M, Samii A (2011) Diffusion tensor imaging-based fiber tracking for prediction of the position of the facial nerve in relation to large vestibular schwannomas. J Neurosurg 115(6):1087–1093. doi:10.3171/2011.7.JNS11495
26. Roundy N, Delashaw JB, Cetas JS (2012) Preoperative identification of the facial nerve in patients with large cerebellopontine angle tumors using high-density diffusion tensor imaging: Clinical article. J Neurosurg 116(4):697–702
27. Mangin JF, Poupon C, Clark C, Le Bihan D, Bloch I (2002) Distortion correction and robust tensor estimation for MR diffusion imaging. Med Image Anal 6(3):191–198
28. Rhoton AL Jr (2000) The cerebellopontine angle and posterior fossa cranial nerves by the retrosigmoid approach. Neurosurgery 47(3 Suppl):S93–129
29. Silverstein H (1984) Cochlear and vestibular gross and histologic anatomy (as seen from postauricular approach). Otolaryngol Head Neck Surg 92(2):207–211
30. Ozdogmus O, Sezen O, Kubilay U, Saka E, Duman U, San T, Cavdar S (2004) Connections between the facial, vestibular and cochlear nerve bundles within the internal auditory canal. J Anat 205(1):65–75. doi:10.1111/j.0021-8782.2004.00313.x
31. Yamakami I, Uchino Y, Kobayashi E, Yamaura A (2003) Computed tomography evaluation of air cells in the petrous bone-relationship with postoperative cerebrospinal fluid rhinorrhea. Neurol Med Chir (Tokyo) 43(7):334–338 discussion 339
32. Yoshino M, Kin T, Saito T, Nakagawa D, Nakatomi H, Kunimatsu A, Oyama H, Saito N (2013) Optimal setting of image bounding box can improve registration accuracy of diffusion tensor tractography. Int J Comput Assist Radiol Surg. doi:10.1007/s11548-013-0934-3
33. Fujiwara S, Sasaki M, Wada T, Kudo K, Hirooka R, Ishigaki D, Nishikawa Y, Ono A, Yamaguchi M, Ogasawara K (2011) High-resolution diffusion tensor imaging for the detection of diffusion abnormalities in the trigeminal nerves of patients with trigeminal neuralgia caused by neurovascular compression. J Neuroimaging 21(2):e102–108. doi:10.1111/j.1552-6569.2010.00508.x

OPEN

Citation: Transl Psychiatry (2014) **4**, e472; doi:10.1038/tp.2014.110

www.nature.com/tp

ORIGINAL ARTICLE

Common variants at 1p36 are associated with superior frontal gyrus volume

R Hashimoto[1,2,13], M Ikeda[3,13], F Yamashita[4], K Ohi[2], H Yamamori[2,5], Y Yasuda[2], M Fujimoto[2], M Fukunaga[6], K Nemoto[7], T Takahashi[8], M Tochigi[9], T Onitsuka[10], H Yamasue[9], K Matsuo[11], T Iidaka[12], N Iwata[3], M Suzuki[8], M Takeda[1,2], K Kasai[9] and N Ozaki[12]

The superior frontal gyrus (SFG), an area of the brain frequently found to have reduced gray matter in patients with schizophrenia, is involved in self-awareness and emotion, which are impaired in schizophrenia. However, no genome-wide association studies of SFG volume have investigated in patients with schizophrenia. To identify single-nucleotide polymorphisms (SNPs) associated with SFG volumes, we demonstrated a genome-wide association study (GWAS) of gray matter volumes in the right or left SFG of 158 patients with schizophrenia and 378 healthy subjects. We attempted to bioinformatically ascertain the potential effects of the top hit polymorphism on the expression levels of genes at the genome-wide region. We found associations between five variants on 1p36.12 and the right SFG volume at a widely used benchmark for genome-wide significance ($P < 5.0 \times 10^{-8}$). The strongest association was observed at rs4654899, an intronic SNP in the eukaryotic translation initiation factor 4 gamma, 3 (*EIF4G3*) gene on 1p36.12 ($P = 7.5 \times 10^{-9}$). No SNP with genome-wide significance was found in the volume of the left SFG ($P > 5.0 \times 10^{-8}$); however, the rs4654899 polymorphism was identified as the locus with the second strongest association with the volume of the left SFG ($P = 1.5 \times 10^{-6}$). *In silico* analyses revealed a proxy SNP of rs4654899 had effect on gene expression of two genes, *HP1BP3* lying 3′ to *EIF4G3* ($P = 7.8 \times 10^{-6}$) and *CAPN14* at 2p ($P = 6.3 \times 10^{-6}$), which are expressed in moderate-to-high levels throughout the adult human SFG. These results contribute to understand genetic architecture of a brain structure possibly linked to the pathophysiology of schizophrenia.

Translational Psychiatry (2014) **4,** e472; doi:10.1038/tp.2014.110; published online 21 October 2014

INTRODUCTION

Schizophrenia is a common and complex psychiatric disorder with a lifetime risk of approximately 1%. This disorder has a strong genetic component; the estimated heritability is 81%.[1] Multiple genetic variants that have a small effect have been implicated in the pathogenesis of schizophrenia.[2] A genome-wide association study (GWAS) of single-nucleotide polymorphisms (SNPs) that accesses tens of thousands of DNA samples from patients and controls can be a powerful tool for identifying common risk factors for complex diseases, such as schizophrenia. GWASs on schizophrenia have identified several genome-wide significant associated variants.[3,4] Subsequently, GWASs on neurobiological quantitative traits as intermediate phenotypes that possibly reflect the underlying genetic vulnerability better than diagnostic categorization, such as schizophrenia,[5,6] have been performed to minimize the clinical and genetic heterogeneity in studies of schizophrenia.[7]

The superior frontal gyrus (SFG) of the brain is frequently found to have reduced gray matter in individuals with first-episode schizophrenia and neuroleptic naive schizophrenia, as well as chronic patients with schizophrenia.[8,9] The SFG is involved in self-awareness and emotion.[10,11] Self-awareness is the cognitive ability to differentiate between self and non-self cues and is necessary to understand the behavior of other humans. Disturbance in self-awareness linked to social cognition is a core feature of schizophrenia.[12] Emotional disturbances, including meaningless laughter, are often observed in patients with schizophrenia. Meaningless laughter was also observed in unaffected siblings of schizophrenia, thus indicating its heritability.[13] In addition, laughter can be elicited by electrical stimulation of the SFG. Gray matter volumes of bilateral SFG have a strong genetic component, with an estimated heritability of 76–80%.[14] As there is considerable inter-individual variation in the degree of reduced volume of the SFG, it appears that genetic influences have a role in determining the degree of volume reduction of the SFG in schizophrenia. Although GWASs of bilateral hippocampal volume have recently been reported,[15,16] no study has investigated other brain areas in patients with schizophrenia. To identify an SNP related to SFG volumes, we conducted a GWAS of gray matter volumes in the right or left SFG of patients with schizophrenia and healthy subjects.

[1]Molecular Research Center for Children's Mental Development, United Graduate School of Child Development, Osaka University, Suita, Osaka, Japan; [2]Department of Psychiatry, Osaka University Graduate School of Medicine, Suita, Osaka, Japan; [3]Department of Psychiatry, Fujita Health University School of Medicine, Toyoake, Aichi, Japan; [4]Division of Ultrahigh Field MRI, Institute for Biomedical Sciences, Iwate Medical University, Yahaba, Iwate, Japan; [5]Department of Molecular Neuropsychiatry, Osaka University Graduate School of Medicine, Suita, Osaka, Japan; [6]Biofunctional Imaging, Immunology Frontier Research Center, Osaka University, Suita, Osaka, Japan; [7]Department of Neuropsychiatry, Institute of Clinical Medicine, University of Tsukuba, Ibaraki, Japan; [8]Department of Neuropsychiatry, Graduate School of Medicine and Pharmaceutical Sciences, University of Toyama, Toyama, Japan; [9]Department of Neuropsychiatry, Graduate School of Medicine, University of Tokyo, Tokyo, Japan; [10]Department of Neuropsychiatry, Graduate School of Medical Sciences, Kyushu University, Fukuoka, Japan; [11]Division of Neuropsychiatry, Department of Neuroscience, Yamaguchi University Graduate School of Medicine, Yamaguchi, Japan and [12]Department of Psychiatry, Nagoya University Graduate School of Medicine, Nagoya, Aichi, Japan. Correspondence: Professor R Hashimoto, Molecular Research Center for Children's Mental Development, United Graduate School of Child Development, Osaka University, D3, 2-2, Yamadaoka, Suita, Osaka 5650871, Japan.
E-mail: hashimor@psy.med.osaka-u.ac.jp
[13]These authors contributed equally to this work.
Received 3 June 2014; revised 4 August 2014; accepted 31 August 2014

MATERIALS AND METHODS

Subjects

We selected 281 patients with schizophrenia (52.0% males, 146 males and 135 females; mean age 36.0 ± 12.4 years) and 413 healthy controls (49.6% males, 205 males and 208 females; mean age 36.4 ± 12.8 years) for a GWAS of schizophrenia-related phenotypes, such as structural brain morphology, neurocognitive function and neurophysiological assessments.[17–19] All of the subjects were biologically unrelated, there were no first- or second-degree relatives, and all were of Japanese descent.[20,21] The subjects were excluded if they had neurological or medical conditions that could potentially affect the central nervous system, such as atypical headaches, head trauma with loss of consciousness, chronic lung disease, kidney disease, chronic hepatic disease, thyroid disease, active cancer, cerebrovascular disease, epilepsy, seizures, substance-related disorders or mental retardation. Patients with schizophrenia were recruited from the Osaka University Hospital. Each patient had been diagnosed by at least two trained psychiatrists according to the criteria from the DSM-IV (Diagnostic and Statistical Manual of Mental Disorders, Fourth Edition) based on the Structured Clinical Interview for DSM-IV. Current symptoms of schizophrenia were evaluated using the positive and negative syndrome scale. Controls were recruited through local advertisements at Osaka University. The healthy subjects were evaluated using the non-patient version of the Structured Clinical Interview for DSM-IV to exclude individuals who had current or past contact with psychiatric services or who had received psychiatric medications.

Superior frontal volumes obtained from the magnetic resonance imaging data were assessed in 158 patients with schizophrenia and 378 healthy subjects. Detailed demographic information is shown in Supplementary Table S1. Mean age and handedness did not differ significantly between the cases and controls ($P > 0.50$); however, the gender ratio, years of education and estimated premorbid intelligence quotient differed significantly between the cases and controls ($P < 0.05$). The ratio of male was higher in patients with schizophrenia compared with the controls. The years of education and estimated premorbid intelligence quotient were significantly lower in patients with schizophrenia compared with the controls. When the genotype groups in the top five SNPs with genome-wide significance of the right SFG volume were compared within the patient and control groups, we found no differences across the demographic variables, except for the gender ratio in the controls (rs6700718, rs1354792, rs10218584, and rs6702110; $P < 0.05$). Written informed consent was obtained from all the subjects after the procedures had been fully explained. This study was performed in accordance with the World Medical Association's Declaration of Helsinki and was approved by the Research Ethical Committee of Osaka University.

Magnetic resonance imaging procedure and extraction of SFG volumes

All magnetic resonance imaging data were obtained using a 1.5-T GE Signa EXCITE system (Tokyo, Japan). A three-dimensional volumetric acquisition of a T1-weighted gradient echo sequence produced a gapless series of 124 sagittal sections using a spoiled gradient-recalled acquisition in the steady state (SPGR) sequence (TE/TR, 4.2/12.6 ms; flip angle, 15°; acquisition matrix, 256 × 256; 1NEX, FOV, 24 × 24 cm; slice thickness, 1.4 mm). We screened all scans and found no gross abnormalities, such as infarcts, hemorrhages or brain tumors, in any of the subjects. Each image was visually examined to eliminate any images with motion or metal artifacts, and the anterior commissure–posterior commissure line was adjusted.[22] MR images were processed with the VBM8 toolbox (http://dbm.neuro.uni-jena.de/vbm/download/) implemented for SPM8 (Wellcome Department of Imaging Neuroscience, University College London, UK, http://www.fil.ion.ucl.ac.uk/spm) running in MATLAB (The Mathworks, Natick, MA, USA) for tissue segmentation and anatomical normalization, as described elsewhere.[23–25] The voxel values of the normalized gray matter images were modulated according to the nonlinear component of the transformation, which resulted in approximating brain-size-adjusted gray matter volumes while preserving local volume changes.[26] Gray matter volumes of the bilateral SFG were then calculated by using the maximum probabilistic atlas using 20 hand-labeled images (Supplementary Figure S1).[27,28]

SNP selection and SNP genotyping

Genotyping was performed using the Affymetrix Genome-Wide Human SNP Array 6.0 (Affymetrix, Santa Clara, CA, USA), according to the manufacturer's protocol. The genotypes were called from the CEL files using Birdseed v2 for the 6.0 chip implemented in the Genotyping Console software (Affymetrix). We then applied the following quality control (QC) criteria to exclude samples: (i) arrays with low QC (< 0.4) according to Birdseed v2 ($N = 0$), (ii) samples for which $< 95\%$ of the genotypes were called ($N = 0$) and (iii) samples in the same family according to $\hat{\pi}$ (> 0.4, $N = 0$). Next, we excluded SNPs that: (i) had low call rates (< 0.95), (ii) were duplicated, (iii) were localized to sex chromosomes, (iv) deviated from Hardy–Weinberg equilibrium in the controls ($P < 0.0001$) or (v) had low minor allele frequencies < 0.05. After all of these exclusions, 517 946 SNPs that underwent QC remained for experimental analysis.

To test for the existence of a genetic structure in the data, we performed a principal component analysis using EIGENSTRAT 3.0 software.[29] Ten eigenvectors were calculated. Genotype information from the JPT (Japanese in Tokyo, Japan), CHB (Han Chinese in Beijing, China), CEU (Utah residents with ancestors from northern and western Europe) and YRI (Yoruba in Ibadan, Nigeria) in HapMap phase III was compared with our data set to check for population stratification (Supplementary Figure S2).

Statistical analyses

Statistical analyses of the demographic variables were performed using PASW Statistics 18.0 software (SPSS Japan, Tokyo, Japan). Differences in the clinical characteristics between patients and controls were analyzed using χ^2 tests for the categorical variables and the Mann–Whitney *U*-test for the continuous variables. Multiple linear regression analysis was performed to compare the gray matter volumes in the right and left SFG regions among genotypes (the number of major alleles; 0, 1 or 2) using PLINK 1.07 software. Diagnosis, age and gender were included as covariates. Quantile–Quantile is listed in Supplementary Figure S3.

RESULTS

We observed associations between five variants (rs4654899, rs6702110, rs6700718, rs10218584 and rs1354792) on 1p36.12 and the right SFG volume at a widely used benchmark for genome-wide significance ($P < 5.0 \times 10^{-8}$, r^2 among SNPs > 0.8; Figure 1). The strongest association was observed at rs4654899, an intronic SNP in the eukaryotic translation initiation factor 4 gamma, 3 (*EIF4G3*) gene on 1p36.12 ($P = 7.5 \times 10^{-9}$; Figure 2). No SNP with genome-wide significance was found in the volume of the left SFG; however, the rs4654899 polymorphism was identified as the locus with the second strongest association with the volume of the left SFG ($P = 1.5 \times 10^{-6}$; Figure 1). The top 10 and top 200 markers on each SFG are shown in Tables 1 and 2 and Supplementary Tables S2 and S3. *Post hoc* analyses separately assessed in patients and controls also revealed reduced but significant associations (Tables 1 and 2 and Supplementary Tables S2 and S3). Genotype effects of rs4654899 on gray matter volume of right superior frontal gyrus were found in patients with schizophrenia and controls (Figure 3). We attempted to bioinformatically ascertain the potential effects of the rs4654899 polymorphism on the expression levels of genes at the genome-wide region by using the mRNA by SNP Browser 1.0.1 database (http://www.sph.umich.edu/csg/liang/asthma/). Significant effects of the rs3767248 proxy SNP for rs4654899 ($r^2 = 1.0$) were identified

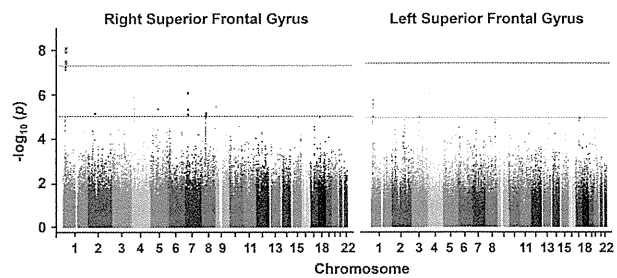

Figure 1. Manhattan plots derived from the multiple linear regression analysis of the bilateral superior frontal volumes. The blue line indicates a *P*-value of 1.0E − 05. The red line indicates a *P*-value of 5.0E − 08.

in the expressions of the heterochromatin protein 1, binding protein 3 (*HP1BP3*) gene ($P=7.8\times10^{-6}$), which lies 3′ to *EIF4G3*, as a cis-acting effect (< 200 kb), and the calpain 14 (*CAPN14*) gene ($P=6.3\times10^{-6}$), as a trans-acting effect (> 200 kb; Supplementary Table S4). Both *HP1BP3* and *CAPN14* are expressed in moderate-to-high levels throughout the adult human SFG (Supplementary Figures S4 and Supplementary Figure S5), as visualized in the Allen Institute Human Brain Atlas Explorer 2 software (http://human.brain-map.org/static/brainexplorer).

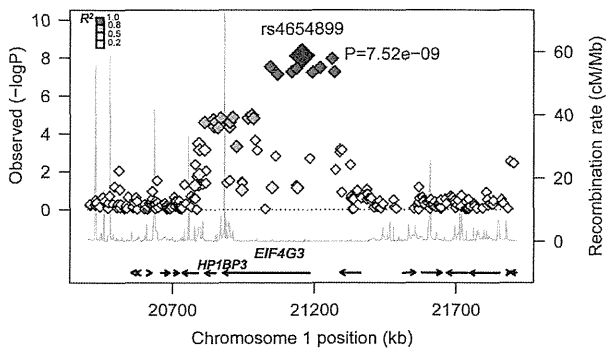

Figure 2. The strongest association with the right superior frontal gyrus was found for rs4654899. *P*-values ($-\log_{10}$) are shown in regions peripheral to rs4654899 (±750 kb).

DISCUSSION

To date, it remained unclear whether there were genetic variants strongly related to SFG volume in patients with schizophrenia and healthy subjects. This study is the first GWAS to identify the SNPs associated with the SFG, which have an important role in schizophrenia-related social functions and is reduced in patients with schizophrenia. We revealed that there were associations at the genome-wide significant level between SFG and genetic variants of the *EIF4G3* gene on 1p36.12. Individuals with minor A-allele of the most significant variant rs4654899 had smaller right SFG volumes compared with those with major C-allele in both patients and controls. Bioinformatical data indicate that the rs3767248 proxy SNP for rs4654899 has important roles in the expression of the *HP1BP3* and *CAPN14* genes, which are expressed in human adult SFG. The *HP1BP3* and *CAPN14* gene expressions of the minor G-allele of the rs3767248 polymorphism were significantly lower than those of the major A-allele. However, whether the expression levels of these genes in the brains or serums of patients with schizophrenia are lower or higher than those in healthy subjects is unknown. Further study is needed to investigate the difference of the expressions between patients and controls.

Table 1. TOP 10 SNPs for the right superior frontal gyrus

Rank	*SNP*	*Chr*	*Bp*	*m*	*M*	*MAF*	*Combined subjects*			*Schizophrenia*			*Controls*			*Closest gene*
							N	*β*	P	*N*	*β*	P	*N*	*β*	P	
1	rs4654899	1	21410231	A	C	0.33	509	−969.5	**7.52E−09**	153	−1164	3.71E−04	356	−935.9	1.86E−06	*EIF4G3*
2	rs6702110	1	21515906	G	A	0.32	526	−965.3	**1.07E−08**	155	−1255	1.79E−04	371	−902.3	4.34E−06	*EIF4G3*
3	rs6700718	1	21299363	A	C	0.33	537	−895.1	**2.89E−08**	159	−1110	4.68E−04	378	−847.7	6.81E−06	*EIF4G3*
4	rs10218584	1	21474480	G	C	0.33	537	−891.8	**3.21E−08**	159	−1110	4.68E−04	378	−842.7	7.68E−06	*EIF4G3*
5	rs1354792	1	21391875	C	T	0.33	535	−892.7	**3.46E−08**	157	−1114	5.35E−04	378	−847.7	6.81E−06	*EIF4G3*
6	rs6703227	1	21374810	C	T	0.33	537	−879.3	5.28E−08	159	−1056	9.55E−04	378	−847.7	6.81E−06	*EIF4G3*
7	rs1609558	1	21525228	C	T	0.30	533	−899.8	5.36E−08	158	−1031	1.18E−03	375	−870.9	7.67E−06	*EIF4G3*
8	rs12402486	1	21447935	A	G	0.34	527	−880.9	5.58E−08	159	−1110	4.68E−04	368	−830	1.20E−05	*EIF4G3*
9	rs2874367	1	21324491	A	C	0.33	531	−874.5	7.19E−08	157	−1092	6.24E−04	374	−829	1.25E−05	*EIF4G3*
10	rs6945071	7	26122423	G	A	0.16	537	−1035	8.46E−07	159	−1120	3.25E−03	378	−983.2	1.02E−04	*NFE2L3*

Abbreviations: Chr, chromosome; Bp, nucleotide location; m, minor allele; M, major allele; MAF, minor allele frequency; SNP, single-nucleotide polymorphism. Genome-wide significant *P*-values are shown as bold font and are underlined.

Table 2. TOP 10 SNPs for the left superior frontal gyrus

Rank	*SNP*	*Chr*	*Bp*	*m*	*M*	*MAF*	*Combined subjects*			*Schizophrenia*			*Controls*			*Closest gene*
							N	*β*	P	*N*	*β*	P	*N*	*β*	P	
1	rs4574391	4	27212223	C	T	0.25	533	−880	7.63E−07	158	−693	4.27E−02	375	−965	3.51E−06	*STIM2*
2	rs4654899	1	21410231	A	C	0.33	509	−787	1.51E−06	153	−691	3.81E−02	356	−863	4.22E−06	*EIF4G3*
3	rs2046701	4	27211040	C	A	0.25	532	−826	2.22E−06	158	−697	3.87E−02	374	−887	1.28E−05	*STIM2*
4	rs1609558	1	21525228	C	T	0.3	533	−763	2.33E−06	158	−524	1.11E−01	375	−885	1.67E−06	*EIF4G3*
5	rs6702110	1	21515906	G	A	0.32	526	−769	3.37E−06	155	−714	3.90E−02	371	−834	9.21E−06	*EIF4G3*
6	rs10218584	1	21474480	G	C	0.33	537	−704	8.32E−06	159	−566	8.48E−02	378	−791	1.05E−05	*EIF4G3*
7	rs1354792	1	21391875	C	T	0.33	535	−704	8.69E−06	157	−625	5.92E−02	378	−776	1.59E−05	*EIF4G3*
8	rs2623384	3	99064220	G	A	0.39	525	−724	9.15E−06	157	−894	6.79E−03	368	−642	5.92E−04	*COL8A1*
9	rs2292343	17	45455670	C	G	0.34	524	−721	9.74E−06	155	−836	1.22E−02	369	−666	3.45E−04	*EFCAB13*
10	rs3883317	17	45484111	A	G	0.34	534	−703	1.03E−05	158	−743	2.70E−02	376	−675	1.72E−04	*EFCAB13*

Abbreviations: Chr, chromosome; Bp, nucleotide location; m, minor allele; M, major allele; MAF, minor allele frequency; SNP, single-nucleotide polymorphism.

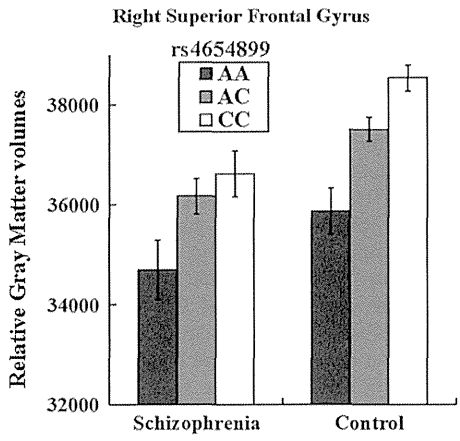

Figure 3. Impact of the rs4654899 genotype of the *EIF4G3* gene on the right superior frontal gyrus. Each column shows relative gray matter volumes of the right superior frontal gyrus. Error bars represent the standard error.

To our knowledge, no study has reported associations between these genes and schizophrenia, although the chromosomal region (1p36.12) related to the risk of schizophrenia has been reported.[30] The exact functions of these two genes are unknown; however, *HP1BP3* is predicted to bind to DNA and have a role in nucleosome assembly. *CAPN14*, which belongs to the calpain large subunit family, is a cytosolic calcium-activated cysteine protease involved in a variety of cellular processes, including apoptosis, cell division, modulation of integrin–cytoskeletal interactions and synaptic plasticity.

In this study, we examined the effects of genotypes on SFG volumes in a combined sample of patients and controls, and found similar effects of genotypes in patients and controls. Susceptibility genes for schizophrenia do not directly encode for their clinical syndrome/behaviors. The syndrome/behaviors observed in schizophrenia are produced by intermediate steps that occur between genes and syndrome/behaviors; and intermediate steps, such as changes of brain volumes, underlie the syndrome/behavior of schizophrenia. The intermediate phenotypes are located on the pathogenesis path, and are likely associated with a more basic and proximal etiological process rather than pathogenesis of disease itself.[5,6] Therefore, each genetic variant is related to controls as well as patients, and accumulations of each genetic variant could contribute to pathogenesis of schizophrenia through intermediate steps.

To date, although abnormal brain lateralization in schizophrenia causing a failure of left hemisphere dominance has been reported,[31] there is no evidence of SFG lateralization in schizophrenia. In addition, there is no report for developmental/functional differences between the right and left SFG. We found genome-wide significant variants related to right SFG volumes, whereas these variants were not related to left SFG volumes at genome-wide significant level. The difference of significance between right and left SFG was due to a difference of genotype effects in patients (for example, rs4654899, right: $P=3.71\times10^{-4}$, left: $P=3.81\times10^{-2}$) but not in controls (right: $P=1.86\times10^{-6}$, left: $P=4.22\times10^{-6}$). As it has been reported that gray matter volume deficits were more extensive in individuals with first-episode schizophrenia and neuroleptic naive than that of their neuroleptic-treated counterparts in left SFG,[9] confounding factors, such as duration of antipsychotic treatment or dose of antipsychotics, might affect our results.

In this study, we provide new insights into the genetic architecture of a brain structure closely linked to schizophrenia. It is still unclear whether and to what extent the effects of the genetic variant on SFG volumes observed here might be associated with an increased risk for schizophrenia. We suggest that the variant may have a role in the impairments of self-awareness and emotion noted in patients with schizophrenia through volumetric vulnerability of the SFG.

There were several limitations to this study. We recruited a relatively large sample with an only Japanese ethnicity to avoid population stratification. However, the existence of a false-positive association cannot be excluded as an explanation for our results. Further investigations of other samples with much larger sample sizes and/or with different ethnicities are needed to confirm our findings. It is unclear whether our results are directly/indirectly linked to the rs4654899 SNP, to other SNPs in high linkage disequilibrium with this SNP or to interactions between this SNP and other SNPs. To determine whether rs4654899 is the most strongly associated variant for SFG volume in the chromosomal region, an extensive search such as sequencing for other functional variants at this locus could provide further information underlying the genomic mechanism for this variant.

In conclusion, we found that genetic variants of the *EIF4G3* gene could be associated with structural vulnerability of the SFG. Further replication studies are necessary to confirm our findings. Identification of causal variants and the functional effects of these genes may help to reveal additional genetic variables involved in the neurodevelopment and pathogenesis of schizophrenia.

CONFLICT OF INTEREST

The authors declare no conflict of interest.

ACKNOWLEDGMENTS

We thank all the individuals who participated in this study. This work was supported by research grants from the Japanese Ministry of Health, Labor and Welfare (H22-seishin-ippan-001); KAKENHI, 22390225-Grant-in-Aid for Scientific Research (B), 23659565-Grant-in-Aid for Challenging Exploratory Research and Grant-in-Aid for Scientific Research on Innovative Areas (Comprehensive Brain Science Network) from the Japanese Ministry of Education, Culture, Sports, Science and Technology (MEXT) and the Japan Foundation for Neuroscience and Mental Health.

REFERENCES

1 Sullivan PF, Kendler KS, Neale MC. Schizophrenia as a complex trait: evidence from a meta-analysis of twin studies. *Arch Gen Psychiatry* 2003; **60**: 1187–1192.
2 Sun J, Kuo PH, Riley BP, Kendler KS, Zhao Z. Candidate genes for schizophrenia: a survey of association studies and gene ranking. *Am J Med Genet B Neuropsychiatr Genet* 2008; **147B**: 1173–1181.
3 Stefansson H, Ophoff RA, Steinberg S, Andreassen OA, Cichon S, Rujescu D *et al.* Common variants conferring risk of schizophrenia. *Nature* 2009; **460**: 744–747.
4 O'Donovan MC, Craddock N, Norton N, Williams H, Peirce T, Moskvina V *et al.* Identification of loci associated with schizophrenia by genome-wide association and follow-up. *Nat Genet* 2008; **40**: 1053–1055.
5 Meyer-Lindenberg A, Weinberger DR. Intermediate phenotypes and genetic mechanisms of psychiatric disorders. *Nat Rev Neurosci* 2006; **7**: 818–827.
6 Tan HY, Callicott JH, Weinberger DR. Intermediate phenotypes in schizophrenia genetics redux: is it a no brainer? *Mol Psychiatry* 2008; **13**: 233–238.
7 Hashimoto R, Ikeda M, Ohi K, Yasuda Y, Yamamori H, Fukumoto M *et al.* Genome-wide association study of cognitive decline in schizophrenia. *Am J Psychiatry* 2013; **170**: 683–684.
8 Chan RC, Di X, McAlonan GM, Gong QY. Brain anatomical abnormalities in high-risk individuals, first-episode, and chronic schizophrenia: an activation likelihood estimation meta-analysis of illness progression. *Schizophr Bull* 2011; **37**: 177–188.
9 Leung M, Cheung C, Yu K, Yip B, Sham P, Li Q *et al.* Gray matter in first-episode schizophrenia before and after antipsychotic drug treatment. Anatomical likelihood estimation meta-analyses with sample size weighting. *Schizophr Bull* 2011; **37**: 199–211.
10 Goldberg II, Harel M, Malach R. When the brain loses its self: prefrontal inactivation during sensorimotor processing. *Neuron* 2006; **50**: 329–339.
11 Fried I, Wilson CL, MacDonald KA, Behnke EJ. Electric current stimulates laughter. *Nature* 1998; **391**: 650.